

# ***CD133 as a Biomarker for an Autoantibody-to-ImmunoPET Paradigm for the Early Detection of Small Cell Lung Cancer***

*Andrew G. Kunihiro<sup>1†</sup>, Samantha M. Sarrett<sup>2,3,4,†</sup>, Kristin J. Lastwika<sup>1,5,†</sup>, Joell L. Solan<sup>1</sup>, Tatyana Pisarenko<sup>5</sup>, Outi Keinänen<sup>2,4</sup>, Cindy Rodriguez<sup>2,4,6</sup>, Lydia R. Taverne<sup>1</sup>, Annette L. Fitzpatrick<sup>7,8</sup>, Christopher I. Li<sup>1</sup>, A. McGarry Houghton<sup>5,9</sup>, Brian M. Zeglis<sup>2,3,4,6,10,\*</sup>, Paul D. Lampe<sup>1,9,\*</sup>*

<sup>1</sup> Translational Research Program, Public Health Sciences Division, Fred Hutchinson Cancer Research Center, Seattle, WA

<sup>2</sup> Department of Chemistry, Hunter College, City University of New York, New York, NY

<sup>3</sup> Ph.D. Program in Biochemistry, City University of New York, New York, NY

<sup>4</sup> Department of Radiology, Memorial Sloan Kettering Cancer Center, New York, NY

<sup>5</sup> Clinical Research Division, Fred Hutchinson Cancer Research Center, Seattle, WA

<sup>6</sup> Ph.D. Program in Biochemistry, City University of New York, New York, NY

<sup>7</sup> Department of Family Medicine, University of Washington, Seattle, WA

<sup>8</sup> Department of Global Health, University of Washington, Seattle, WA

<sup>9</sup> Human Biology Division, Fred Hutchinson Cancer Research Center, Seattle, WA

<sup>10</sup> Department of Radiology, Weill Cornell Medical College, New York, NY

<sup>†</sup>These authors contributed equally to this work.

**First Authors:** Andrew G. Kunihiro, Fred Hutchinson Cancer Research Center, Seattle, WA, USA, email: [akunihir@fredhutch.org](mailto:akunihir@fredhutch.org) — Samantha M. Sarrett, City University of New York, New York, NY, USA, email: [samanthasarret@live.com](mailto:samanthasarret@live.com) — Kristin Lastwika, Fred Hutchinson Cancer Research Center, Seattle, WA, USA, email: [klastwika@fredhutch.org](mailto:klastwika@fredhutch.org).

**Corresponding Authors:** Brian M. Zeglis, 413 East 69<sup>th</sup> Street, New York, NY, 10021, email: [bz102@hunter.cuny.edu](mailto:bz102@hunter.cuny.edu); Paul D. Lampe, 1100 Fairview Ave. N., Seattle, WA 98109, email: [plampe@fredhutch.org](mailto:plampe@fredhutch.org).

**Word Count (including references):** 5,535

**Running Title:** CD133-Targeted ImmunoPET in SCLC

**Keywords:** SCLC, CD133, immunoPET, autoantibody

**Disclosure:** No potential conflicts of interest relevant to this article exist

## ABSTRACT

Small cell lung cancer (SCLC) is a deadly neuroendocrine tumor for which there are no screening methods sensitive enough to facilitate early, effective intervention. We propose targeting the neuroendocrine tumor neoantigen CD133 via antibody-based early detection and positron emission tomography (immunoPET) to facilitate the earlier and more accurate detection of SCLC.

**Methods:** RNAseq datasets, IHC, flow cytometry, and western blots were used to quantify CD133 expression in healthy and SCLC patients. CD133 was imaged *in vivo* using near-infrared fluorescence immunoimaging and zirconium-89 immunoPET. Anti( $\alpha$ )-CD133 autoantibody levels were measured in SCLC patient plasma using antibody microarrays.

**Results:** Across 6 publicly available datasets, CD133 mRNA was found to be higher in SCLC tumors compared to other tissues, including healthy or normal adjacent lung and non-SCLC samples. Critically, the upregulation of CD133 mRNA in SCLC was associated with a significant increase (HR 2.62) in death. CD133 protein was expressed in primary human SCLC, in SCLC patient-derived xenografts (PDXs), and in both SCLC cell lines tested (H82 and H69). Using a H82 xenograft mouse model, we first imaged CD133 expression with near-infrared fluorescence (NIRF). Both *in vivo* and *ex vivo* NIRF clearly show that a fluorophore-tagged  $\alpha$ CD133 homed to lung tumors. Next, we validated the non-invasive visualization of subcutaneous and orthotopic H82 xenografts via immunoPET. An  $\alpha$ CD133 antibody labeled with the positron-emitting radiometal zirconium-89 demonstrated significant accumulation in tumor tissue while producing minimal uptake in healthy organs. Finally, plasma  $\alpha$ CD133 autoantibodies were found in subjects from cohort studies up to 1 year prior to SCLC diagnosis.

**Conclusion:** In light of these findings, we conclude that the presence of  $\alpha$ CD133 autoantibodies in a blood sample followed by CD133-targeted  $^{89}\text{Zr}$ -immunoPET could be an effective early detection screening strategy for SCLC.

## INTRODUCTION

Most small cell lung cancer (SCLC) diagnoses are made at the extensive-stage of the disease after metastases are widely distributed. Despite initial response to etoposide and cisplatin, the median survival for extensive-stage SCLC is only 8-12 months. While SCLC has a dismal 5-year survival rate of <3% for extensive-stage, this improves to nearly 50% if diagnosed at limited-stage disease when treatments can be curative (1,2). Unfortunately, the annual low-dose computed tomography recommended for heavy smokers (who comprise 90% of SCLC cases) is unreliable for detecting limited-stage SCLC (1,3). Other modalities, like fluorodeoxyglucose-positron emission tomography (FDG-PET), are also ineffective for identifying limited-stage disease (4). More advanced imaging methods — such as antibody-based PET (immunoPET) — offer higher specificity than FDG-PET and increased spatial resolution compared to low-dose computed tomography and could thus detect and locate even small SCLC lesions, allowing for effective therapeutic interventions (5).

CD133 is a glycoprotein expressed in many tumor types (including SCLC) that is often used as a marker for cancer stem cells (6,7). These cells, which have been imaged using an anti-CD133 monoclonal antibody conjugated immunomagnetic nanosensor (8), are thought to drive tumor initiation, suggesting that CD133 upregulation occurs early in tumorigenesis and may thus be useful for early screening. CD133 is also associated with chemo- and radiotherapy resistance in SCLC cell lines and patient samples indicating the functional relevance of its expression (9,10). While CD133-positive tumors as small as 2 mm have been successfully imaged via immunoPET in preclinical models of cancers with poor prognoses (e.g. aggressive variant prostate cancer, colon cancer, and glioma), the utility of screening for SCLC by CD133-targeted immunoPET has yet to be explored (6,11-13).

Given the acute and unmet need for the early detection of SCLC, this investigation is focused on the creation of a novel diagnostic platform for the disease predicated on targeting CD133. To this end, we illustrated the feasibility of SCLC-specific imaging by comparing the expression of CD133 in healthy tissue vs SCLC and other lung tumors, performed near-infrared fluorescence and immunoPET imaging of CD133 in murine models of SCLC as a proof-of-concept for *in vivo* detection, and demonstrated that autoantibodies against CD133 are elevated a year before primary SCLC diagnosis but are not present in patients with colon, pancreas, or non-small cell lung cancer. Ultimately, we propose that CD133 could form the basis of a non-invasive ‘autoantibody-to-immunoPET’ paradigm that could be added to current lung cancer screening programs.

## MATERIALS AND METHODS

### CD133 Expression

Surface expression of CD133 was determined by flow cytometry: The human SCLC cell lines NCI-H82 and NCI-H69, purchased from ATCC, were incubated with a live/dead stain, then anti-CD133 antibody (HB#7, Developmental Studies Hybridoma Bank), followed by anti-IgG-AF647 (#A31571), and analyzed using a FACSCanto II (BD Bioscience).

Human tissue microarrays (TMAs) of healthy organs (#FDA999-1, n = 33 organs/person from 3 persons; US Biolab) or SCLC cores (#RLN681A, n=62 unique cases (60 were of sufficient quality for evaluation) and n = 6 unique normal adjacent lung) were stained for CD133 (CST #64326) using the automated Bond RX system (Leica). Mouse lungs were formalin-fixed, paraffin-embedded, and sectioned onto glass slides. Adjacent sections were hematoxylin & eosin stained or imaged stain-free on an Odyssey CLx for  $\alpha$ CD133-CF770.

SCLC RNA Sequencing (RNAseq) data was procured from the Gene Expression Omnibus (GEO) and outlined in Supplemental Tables 1 and 2. Expression data and somatic mutations were also analyzed from the Cancer Cell Line Encyclopedia (CCLE) using the DepMap Public 21Q3 dataset, or SCLC patient sample as described in Supplemental Table 3 by George *et al.* (14).

### Small Animal Imaging

All work was approved by local IACUCs and performed following anesthetization with a 2% isoflurane/oxygen mixture. Six-to-eight-week-old female athymic mice (JAX #007850 or #002019) were injected with  $3\text{-}5 \times 10^6$  H82 cells for flank xenografts. For orthotopic xenografts,  $2\text{-}5 \times 10^6$  H82 or H82-*luc* cells were percutaneously injected into the parenchyma of the left lung. The tumors reached an acceptable size for imaging and biodistribution studies ( $\sim 50\text{-}100$  mm<sup>3</sup>) after 2-4 weeks.

MRI was performed on a 1.0T ICON system (Bruker BioSpin) running ParaVision (v6.0.1) with image reconstruction in Osirix Lite (v11.03). For NIRF imaging, mice bearing H82 tumors were injected retro-orbitally with  $\alpha$ CD133 mAb (HB#7) conjugated to the near-infrared fluorophore CF770 (#92222, Biotium) —  $\alpha$ CD133-CF770 (50  $\mu$ g) — 3-4 weeks after cell inoculation. NIRF imaging was performed up to 4 days after  $\alpha$ CD133-CF770 injection, using an IVIS Spectrum with Living Image v4.7.2 (Perkin Elmer). Lungs were excised after terminal *in vivo* imaging and re-imaged *ex vivo*.

PET images of the mice bearing subcutaneous xenografts were acquired using a microPET Focus 120 (Siemens Medical Solutions) (15). Mice underwent static scans between 24 and 144 h after the intravenous tail vein administration of either [<sup>89</sup>Zr]Zr-DFO- $\alpha$ CD133 (3.7-3.9 MBq, 10-10.5  $\mu$ g) or [<sup>89</sup>Zr]Zr-DFO-hIgG<sub>1</sub> (3.3-3.5 MBq, 36-38  $\mu$ g) for a total scan time of 10-30 minutes, with images analyzed using ASIPro VMTM

(Concorde Microsystems). Following terminal PET and euthanasia, the activity concentrations in 15 relevant organs were quantified using an  $^{89}\text{Zr}$ -calibrated Wizard<sup>2</sup>  $\gamma$ -counter (PerkinElmer).

### **Autoantibody Microarrays**

Autoantibody-antigen complexes were analyzed in SCLC patient plasma from the Cardiovascular Health Study (CHS; ancillary study #132) and the Prostate, Lung, Colorectal, and Ovarian (PLCO; study #170) Screening Trial (16-18). We included 22 cases and 34 controls from CHS, and 40 SCLC with 76 controls from PLCO (Supplemental Table 3). Briefly, antibody microarrays were printed in-house, incubated with plasma, probed with anti-human IgG-SeTau647 or IgM-DyLight550 antibody, and imaged on a GenePix 4200A scanner with GenePix Pro 6.0 (Molecular Devices).

### **Statistics**

Figures and statistics were prepared using RStudio (v1.4.1717). Where appropriate, t-tests or ANOVA with post-hoc analyses were performed.

Additional details can be found in the supplemental methods.

## **RESULTS**

### **CD133 is Overexpressed in Limited Stage SCLC Compared to Normal Tissues and Other Lung Tumors**

Since the upregulation of CD133 has previously been reported in several tumor types but has not been uniquely examined in SCLC (6,7,19), we explored this relationship by analyzing publicly available RNAseq datasets. In a cohort of Japanese SCLC patients, the mean expression of CD133 was 5-fold higher than the mean expression across 43 organ samples (Figures 1A and 1E). CD133 expression was also elevated in H209 (4.7-fold) and DMS53 (20.2-fold) SCLC cell lines relative to other healthy tissues. Our immunohistochemical CD133 staining of a healthy-organ microarray showed high concordance between mRNA transcript levels and protein expression (Figure 1B). Most normal tissues were negative for both CD133 mRNA and protein expression and thus are not expected to interfere with the imaging of lung tumors.

In a publicly available, commercially procured patient cohort (Supplemental Table 1), CD133 transcript levels were 2.64-fold greater in SCLC tumors compared to normal lung tissue (Figure 1C). Based on our analysis, CD133 was transcribed regardless of SCLC staging (Supplemental Figures 1A and 2) and was higher in SCLC compared to adenocarcinoma (3.34-fold) or squamous cell carcinoma (5.35-fold) (Figure 1B). In two additional cohorts, we found CD133 was 3.7 to 5.0-fold higher in SCLC tissue than adjacent

healthy tissue (Figure 1B and Supplemental Figure 1C). We also found that high CD133 transcript levels (6.34 mean log<sub>2</sub> expression cut-point) were significantly associated with a 2.62-fold (95% CI: 1.03-6.69) increased risk of death in a cohort of Chinese SCLC patients (Supplemental Figure 1D).

Flow cytometry confirmed that both SCLC cell lines expressed CD133 on the cell surface (Figure 2A). Additionally, two of the four SCLC PDXs displayed appreciable CD133 expression by immunoblotting (data not shown). In a TMA containing cores from 60 SCLC cases and 6 normal adjacent lung tissues, CD133 was specifically expressed in 58% of the SCLC cores but not in any normal adjacent lung tissue, suggesting *in vivo* imaging of CD133 focused on the lungs will have little background signal in normal lung tissue (Figure 2B). Finally, the expression of CD133 does not appear to be dependent on diagnostic stage, underscoring its potential for identifying limited-stage SCLC (Supplemental Figure 2).

### **CD133 is Associated with ASCL1 and POU2F3 Subtypes**

While SCLC is historically categorized as a neuroendocrine tumor (ASCL1 or NEUROD1 expression), more recent classification approaches have also identified non-neuroendocrine (YAP1 or POU2F3 expression) lineages in a fraction (<20%) of SCLC tumors (20). A heatmap comparing expression of CD133 and these four canonical SCLC molecular subtype markers was generated from publicly available data (Figure 3). CD133 expression was primarily localized in the ASCL1-positive cluster (SCLC-A) — the largest cluster identified (61/149) — and ASCL1 was the primary driver of CD133 expression (Supplemental Figures 3 and 4). The other neuroendocrine cluster, NEUROD1-positive (SCLC-N, 28/149), did not have high levels of CD133 expression. Interestingly, a CD133- and POU2F3-positive cluster (SCLC-P, 36/149) suggested that CD133 may also be useful for identifying a non-neuroendocrine subtype of SCLC. Taken together, these data underscore the utility of using CD133 to identify most SCLC including both neuroendocrine and non-neuroendocrine subtypes.

### **A Fluorophore-Tagged $\alpha$ CD133 Antibody can Identify both Subcutaneous and Orthotopic SCLC Tumors *In Vivo***

Using NIRF imaging, we demonstrated that an  $\alpha$ CD133 antibody labeled with a near-infrared fluorophore —  $\alpha$ CD133-CF770 — effectively delineated subcutaneous H82 flank xenografts in female Fox1<sup>tm</sup> nude and NSG mice (Supplemental Figures 5A-C). NSG mice were also inoculated with H82 cells in the left lobe of the lung to form orthotopic tumors (Supplemental Figures 5D-F). After 2-4 weeks, these orthotopic tumors were imaged via  $\alpha$ CD133-CF770 NIRF imaging, producing visible signal emanating from the left lung (Figure 4A and Supplemental Figure 5G). At the end of the experiment, the lungs were harvested and *ex vivo* NIRF imaging confirmed that the signal derived from the orthotopic, left-lobe tumor (Figure 4B). Following histological processing of the lung, H&E staining confirmed tumor growth in the

left lobe (Figure 4C), while *ex vivo* NIRF imaging of adjacent sections co-localized with the H&E (Figure 4D), confirming that the *in vivo* NIRF signal was from the orthotopic tumor.

### **SCLC Tumors can be Delineated via ImmunoPET Using $^{89}\text{Zr}$ -labeled $\alpha\text{CD133}$**

Having illustrated the feasibility of visualizing CD133 expression *in vivo* using immunoNIRF, we next turned to the creation of a more clinically-relevant immunoPET probe. To this end, the same  $\alpha\text{CD133}$  mAb was modified with the chelator desferrioxamine (DFO) via the stochastic ligation of *p*-SCN-Bn-DFO to the lysines of the immunoglobulin (Supplemental Figure 6). MALDI-ToF spectrometry revealed that the resulting immunoconjugate — DFO- $\alpha\text{CD133}$  — boasted a degree of labeling of  $2.2 \pm 0.4$  DFO/mAb (Supplemental Figure 7). DFO- $\alpha\text{CD133}$  was then radiolabeled with the positron-emitting radiometal zirconium-89 ( $^{89}\text{Zr}$ ;  $t_{1/2} = 3.3$  d) to create a radioimmunoconjugate, [ $^{89}\text{Zr}$ ]Zr-DFO- $\alpha\text{CD133}$ , in >99% radiochemical purity that remained >95% intact in human serum over 5 d at 37 °C (Supplemental Figure 8). An immunoreactivity assay with CD133-expressing H82 human SCLC cells revealed that the radioimmunoconjugate boasted an immunoreactive fraction of >0.75. In contrast, a complementary immunoreactivity assay with CD133-negative K562 cells clearly demonstrated that the radioimmunoconjugate did not bind cells absent its target antigen (Supplemental Figure 9) (21).

With these radioimmunoconjugates in hand, we next evaluated their *in vivo* behavior in a xenograft mouse model of SCLC. To this end, female athymic nude mice bearing subcutaneous flank H82 tumors were administered [ $^{89}\text{Zr}$ ]Zr-DFO- $\alpha\text{CD133}$  (3.7 -3.9 MBq, 10-10.5  $\mu\text{g}$ ) or [ $^{89}\text{Zr}$ ]Zr-DFO- hIgG<sub>1</sub> (3.3-3.5 MBq, 36-38  $\mu\text{g}$ ) via intravenous tail-vein injection. The *in vivo* behavior of these radioimmunoconjugates was then assessed via the acquisition of static PET images 24, 72, 120, and 144 h after i.v. administration. The images clearly showed the accumulation of radioactivity signal in the tumor tissue over time, with the tumoral activity concentrations reaching >40 %ID/g (Figure 5A, Supplemental Figure 10, and Supplemental Table 4). A concomitant decrease in signal was observed in all healthy organs over the course of the experiments, ultimately leading to images with very high tumor-to-background contrast.

A terminal biodistribution analysis was performed after the final imaging timepoint to quantify the uptake of [ $^{89}\text{Zr}$ ]Zr-DFO- $\alpha\text{CD133}$  and compare it to that of [ $^{89}\text{Zr}$ ]Zr-DFO-hIgG<sub>1</sub> (Figure 5B and Supplemental Table 5). These data largely mirrored the PET data. A stark difference in the tumoral activity concentrations of the two radioimmunoconjugates was observed:  $50.8 \pm 7.7$  %ID/g for [ $^{89}\text{Zr}$ ]Zr-DFO- $\alpha\text{CD133}$  and  $5.8 \pm 4.0$  %ID/g for [ $^{89}\text{Zr}$ ]Zr-DFO-hIgG<sub>1</sub> — reinforcing the the specificity of the former. The vast majority of healthy tissues displayed <5 %ID/g of [ $^{89}\text{Zr}$ ]Zr-DFO- $\alpha\text{CD133}$ , with only the blood ( $10.1 \pm 1.9$  %ID/g) presenting a value above this level at 144 h post-injection. Both the imaging and biodistribution data demonstrated very low accretion in the tissues normally associated with the metabolism and clearance of  $^{89}\text{Zr}$ -labeled radioimmunoconjugates: the liver, spleen, and bone. Finally, PET imaging

experiments in mice bearing orthotopic H82-*luc* SCLC xenografts in the parenchyma of the left lung yielded promising results as well (Figure 5C and Supplemental Figure 11). The radioimmunoconjugate clearly visualized the tumor tissue and provided images with high tumor-to-background (and especially tumor-to-healthy lung) contrast. Autoradiography of the left (tumor-bearing) and right (healthy) lungs underscored the dramatic difference in radioactivity in each tissue (Figure 5D).

### **$\alpha$ CD133 Autoantibodies are Upregulated in Plasma up to 1 year Prior to Diagnosis of SCLC**

Though we have clearly demonstrated the utility of CD133 as a target for SCLC imaging, several factors (including cost, equipment availability, and radiation exposure) limit the feasibility of diagnostic PET scans for all patients at risk for developing SCLC. Therefore, we posited a blood-based assay to screen high-risk individuals for CD133 would be necessary for the realistic clinical implementation of CD133-targeted immunoPET in SCLC patients. Anti-tumor autoantibodies — such as those resulting in paraneoplastic syndromes (22) — can be elevated during the very early stages of cancer, sometimes even preceding clinical diagnoses by many months or years (23). We therefore determined the presence of  $\alpha$ CD133 autoantibody-antigen complexes in the plasma of patients later diagnosed with SCLC within 1 year of a blood draw as well as controls matched by age, sex, and smoking status (*i.e.*, case-control design) from the CHS and PLCO cohorts. In both cohorts, those later diagnosed with SCLC were significantly more likely than controls to have circulating autoantibodies bound to CD133 (Figure 6A). Given that subject samples were drawn at different times prior to SCLC diagnosis, we measured both early-response IgM and later-produced IgG isotypes. Using a standardized log<sub>2</sub> odds ratio cutoff (0.73) that maximized sensitivity and specificity, we found that 5 SCLC cases had both IgG and IgM autoantibodies, 8 had only IgM, 7 had only IgG, and 11 (35%) had no  $\alpha$ CD133 autoantibodies (Figure 6B) yielding an overall sensitivity of 65% at 71% specificity. Importantly,  $\alpha$ CD133 autoantibodies were elevated in SCLC but not in the other tumors we have tested (*e.g.* colon, pancreas, non-SCLC) (Supplemental Figure 11).

## **DISCUSSION**

While heavy smokers already fall within the lung cancer screening guidelines, a retrospective analysis of the National Lung Screening Trial showed that only 34% of SCLC cases were detected by a scheduled screen. Moreover, stage I/II cancers — for which therapies are most effective — were only discovered with very small nodules (3-7 mm) that unfortunately comprised only 15% of all those detected by the screening (~85% were at more advanced stages). In contrast, all nodules  $\geq 7$  mm had already progressed to stage III/IV (5). A search of the literature uncovered only 4 imaging agents for SCLC currently in development, with none being leveraged as screening tools (24-28). Yet the identification of highest risk populations within those already attending annual lung cancer screens as candidates for non-invasive molecular imaging could

help detect smaller, treatable tumors. In this study, we have identified CD133 as a novel antigen that is upregulated even in limited stage SCLC and have developed a CD133-targeted  $^{89}\text{Zr}$ -immunoPET probe that can delineate tumor tissue with high contrast in murine models of SCLC.

We found CD133 was consistently correlated with ASCL1 and POU2F3 but not YAP1 or NEUROD1 molecular subtypes of lung cancer. This aligns with a prior report that ASCL1 can transcriptionally regulate CD133 expression and increase tumorigenicity in SCLC cells and mouse xenograft models (29). However, this is the first report of an association between CD133 and POU2F3 in SCLC. As POU2F3 is a master regulator of tuft cells (30) and ASCL1 drives neuroendocrine cells, CD133 may be useful for the detection of both neuroendocrine and non-neuroendocrine SCLC. Overall, we found CD133 expression at the transcript and protein levels in approximately 60% of SCLC cases examined. Interestingly, our  $\alpha\text{CD133}$  autoantibody biomarkers mirror this prevalence with a sensitivity of 65%. Current research is ongoing to identify additional autoantibodies or markers needed to capture all SCLC cases.

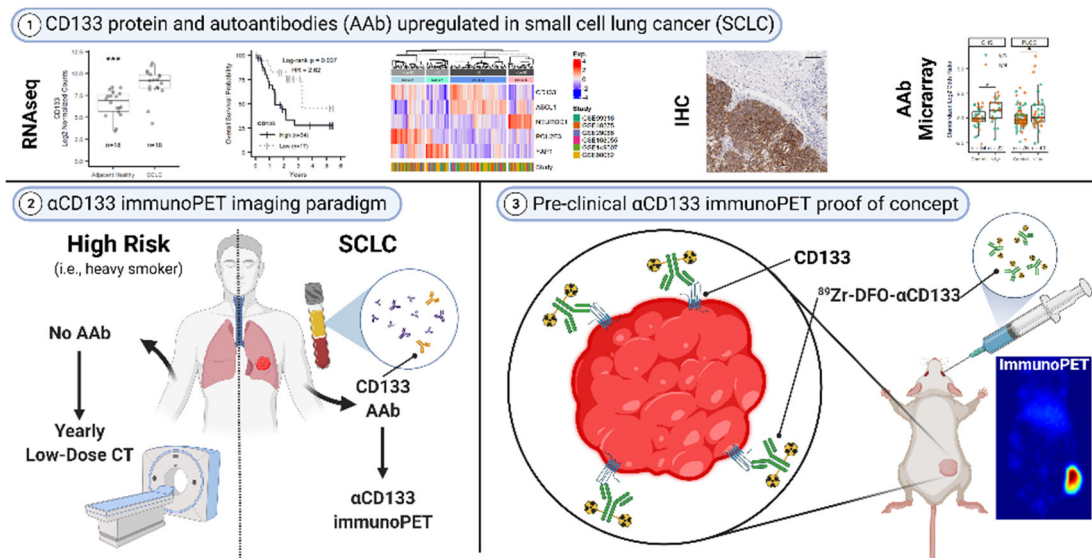
While CD133 is expressed in other types of cancer, we do not believe this would interfere with CD133-targeted SCLC imaging because immunoPET would only be triggered when  $\alpha\text{CD133}$  autoantibodies that indicate SCLC are present in the blood, and  $\alpha\text{CD133}$  autoantibodies are not elevated in other major cancers (Supplemental Figure 12). The case for CD133-targeted immunoPET in SCLC is strengthened by the low levels of CD133 expression in healthy thoracic organs (*e.g.* the lungs, heart, and thymus), suggesting that PET focused on the lungs and mediastinal region should allow for the effective spatial resolution of early, intrathoracic tumors for which therapeutic interventions are possible. Importantly, *in vivo* blocking of [ $^{89}\text{Zr}$ ]Zr-DFO- $\alpha\text{CD133}$  by endogenous autoantibodies is unlikely, as we did not detect human IgG in a tissue microarray containing 45 SCLC tumors (Supplemental Figure 13) but did see extensive staining of SCLC tissue with the  $\alpha\text{CD133}$  antibody (Figure 2). Finally, the shedding of CD133 is unlikely to impede its viability as an imaging target, as  $^{89}\text{Zr}$ -immunoPET probes against several shed antigens — most notably VEGF-A and CA19.9 — have been effectively deployed in the clinic (31,32).

While the goal of this study was to assess CD133 as a target for early SCLC detection via immunoimaging, CD133 may also serve as a therapeutic target. Indeed, the presence of autoantibodies in pre-diagnostic cohorts of SCLC argue that CD133 may be a good target for early intervention with immunotherapy. In fact,  $\alpha\text{CD133}$  immunotherapies and antibody-drug conjugates have shown promise for increasing survival in preclinical models of glioma and myeloid leukemia as well as colorectal, hepatocellular, and gastric cancers (33-38). Phase I/II human trials of  $\alpha\text{CD133}$  chimeric antigen receptor T-cells (CAR-T) have also shown improvements in remission or stable disease for an array of malignancies (39-41).

## CONCLUSION

In the preceding pages, we have clearly demonstrated the increased transcription of CD133 mRNA in SCLC tumors and the over-expression of CD133 protein in SCLC cell lines, PDXs, and primary tumor samples. In addition, we have illustrated that CD133-targeted molecular imaging probes can delineate SCLC xenografts via both NIRF and immunoPET. Finally, we discovered that elevated levels of IgM and IgG autoantibodies against CD133 are present in the blood of SCLC patients up to a year before diagnosis. Supported by these data, we envision the creation of a novel two-tiered  $\alpha$ CD133 ‘autoantibody-to-immunoPET’ early detection paradigm in which a plasma-based biomarker could serve as a companion diagnostic to select patients for the non-invasive molecular imaging of SCLC.

## GRAPHICAL ABSTRACT



## DISCLOSURE

We are grateful for support from the NIH (P50CA228944, R01CA243328, R01CA186157, U01CA185097 to PDL, AMH; R01CA240963, U01CA221046, R01CA204167, R21EB030275, and R01CA244327 to BMZ; F32CA261055 and T32CA009657 to AGK; KL2TR002317 to KJL; R25GM086304 to LRT; and P30CA015704 to the FHCRC/UW Cancer Consortium) and the Academy of Finland (331659 to OMK). CHS samples were used with support from HHSN268201200036C, HHSN268200800007C, HHSN268201800001C, N01HC55222, N01HC85079, N01HC85080, N01HC85081, N01HC85082, N01HC85083, N01HC85086, 75N92021D00006, and U01HL080295 and U01HL130114 from the NHLBI, additional contribution from the NINDS, and by R01AG023629 from the NIA. A full list of principal CHS investigators and institutions can be found at CHS-NHLBI.org.

## **KEY POINTS**

**Question:** Is CD133 a promising biomarker for the early detection and diagnostic immunoPET of SCLC?

**Pertinent Findings:** CD133 mRNA and protein levels are elevated in SCLC tumors, and autoantibodies against CD133 are present in SCLC patients up to a year prior to diagnosis. ImmunoPET with a <sup>89</sup>Zr-labeled CD133-targeted radioimmunoconjugate effectively delineates SCLC tissue in murine models of the disease.

**Implications for Patient Care:** The development of a CD133-targeted early detection and imaging strategy for SCLC will help identify high-risk patients with limited-stage disease and thus facilitate early therapeutic interventions.

## FIGURES AND FIGURE CAPTIONS

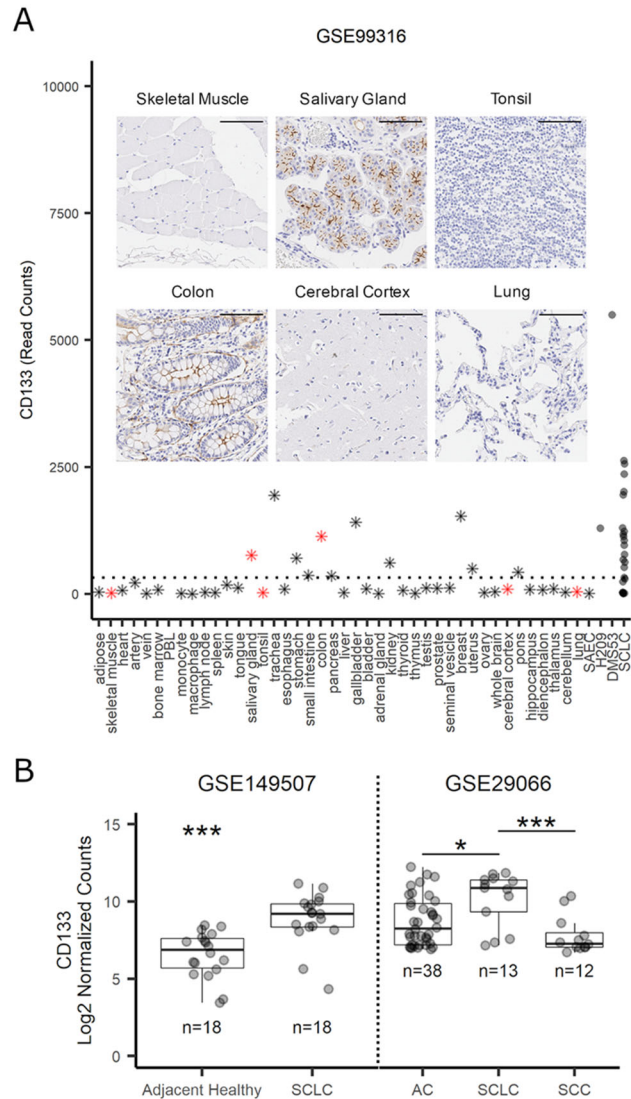


**FIGURE 1.** Expression of CD133 in normal tissue and SCLC. A) RNAseq data for CD133 in healthy organs ( $n = 42$ ), SAEC ( $n = 1$ ), SCLC cell lines ( $n = 2$ ), and SCLC patient tumors ( $n = 23$ ); PBL, peripheral blood leukocytes; SAEC, small airway epithelial cell. The dashed line represents the average expression across all healthy tissue/organs (exclusive of H209, DMS53, and SCLC). Inset shows CD133 protein IHC staining (brown) at 20 $\times$  in tissue microarrays from selected normal tissues (red stars in A; scale=100  $\mu$ m). B) Representative expression levels of CD133 mRNA, from publicly available cohorts, in adjacent healthy or tumor tissue from SCLC patients and between SCLC, adenocarcinoma (AC), or squamous cell carcinoma (SCC) tumors. \*\*  $p < 0.01$ , \*\*\*  $p < 0.001$  by t-test or one-way ANOVA with Tukey adjustment.

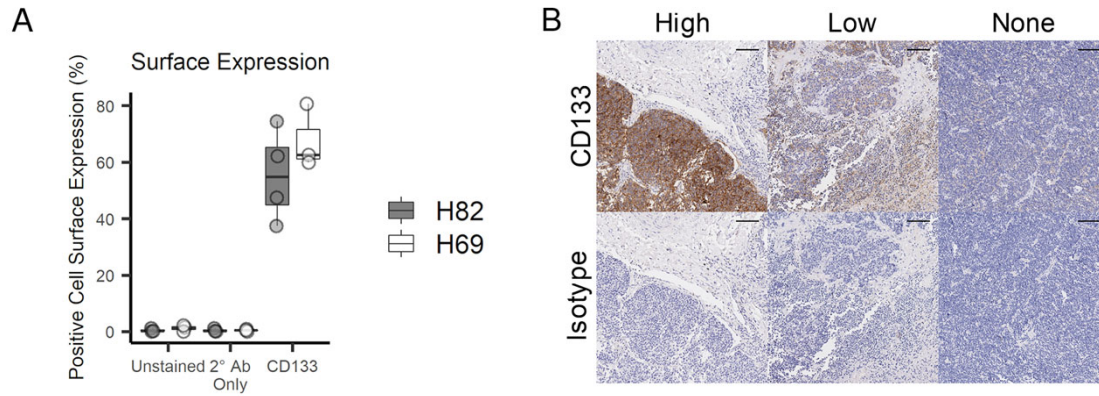


**FIGURE 2.** Characterization of the expression of CD133 protein in SCLC. A) Flow-cytometric detection of CD133 expression in H82 and H69 SCLC cell lines (n = 4 experimental replicates/cell line) B) Representative images of high, low, or absent CD133 expression (top; brown staining) or isotype control (bottom) from a SCLC TMA (scale = 100  $\mu$ m).

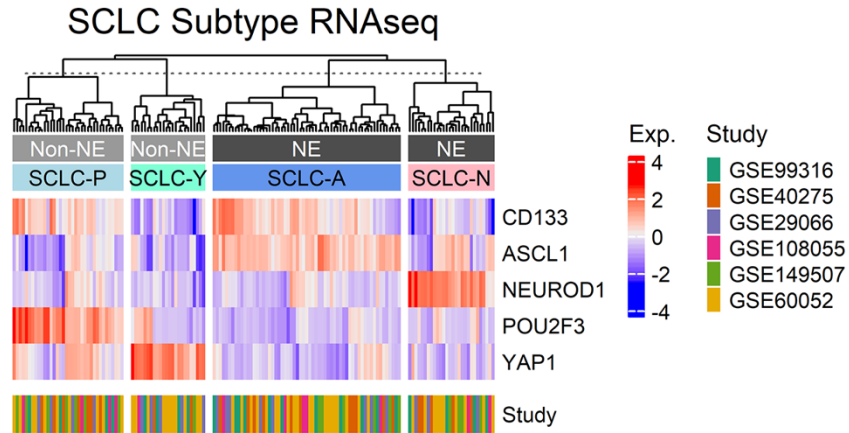


**FIGURE 3.** Clustering of CD133 expression and subtype markers in SCLC. RNAseq data from SCLC GEO data was used to construct a heatmap of CD133 and SCLC subtype marker expression using the ComplexHeatmap R package with clustering using the Ward.D2 method. Z-score of expression was calculated using the *scale* function in R. The Clusters are labeled by their characteristic (neuroendocrine [NE] or non-neuroendocrine [Non-NE]) and by subtype (SCLC-A/N/P/Y).

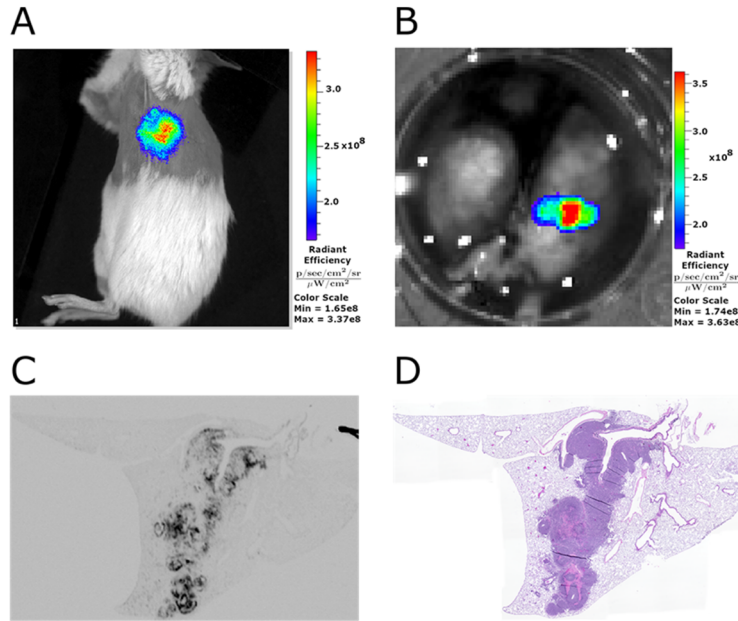


**FIGURE 4.** Near-infrared fluorescence imaging of CD133 in SCLC. A) Representative *in vivo* NIRF imaging of an orthotopic H82 lung tumor in a female NSG mouse following the administration of  $\alpha$ CD133-CF770. B) *Ex vivo* NIRF imaging of the excised lungs from the mouse in panel A. C) H&E and D) NIRF imaging of adjacent histological sections from the same lung shown in panels A and B.

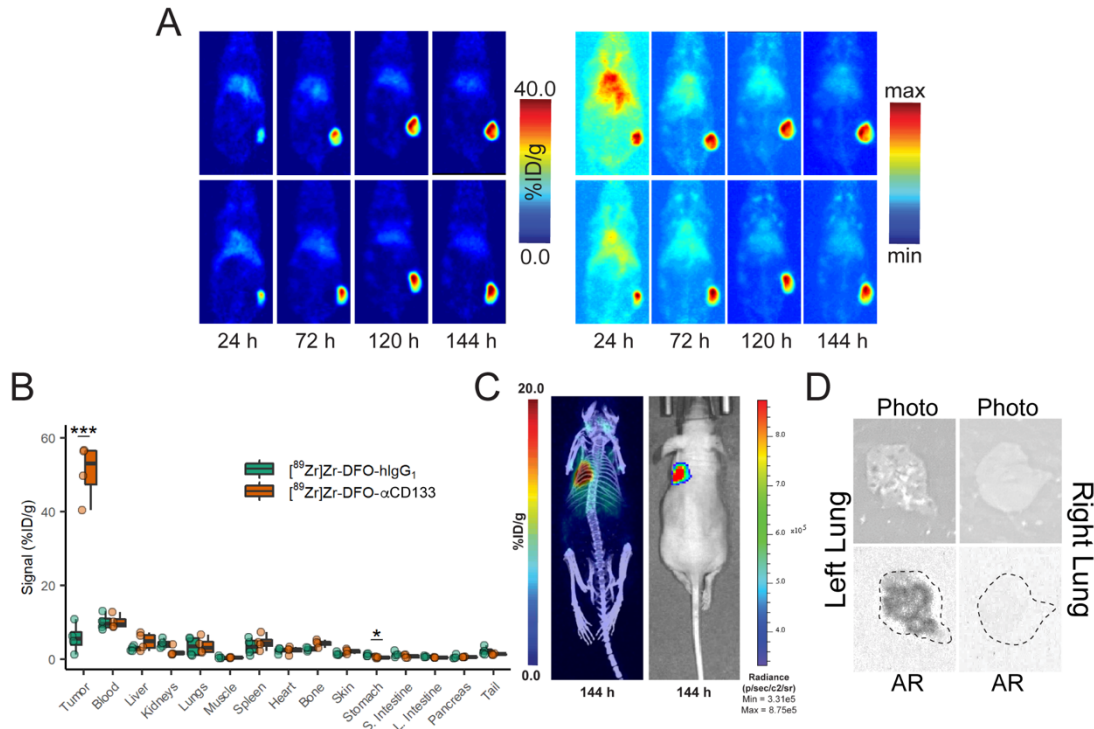


**FIGURE 5.** The *in vivo* validation of  $[^{89}\text{Zr}]\text{Zr-DFO-}\alpha\text{CD133}$ . (A) Representative coronal slice (left) and maximum intensity projection (right) PET images acquired 24, 72, 120, and 144 h after the *i.v.* administration of  $[^{89}\text{Zr}]\text{Zr-DFO-}\alpha\text{CD133}$  (3.7-3.9 MBq, 10-10.5  $\mu\text{g}$ ) to athymic nude mice ( $n = 4$ ) bearing subcutaneous H82 xenografts (150-200  $\text{mm}^3$  at the time of injection). (B) Biodistribution data acquired 144 h after the *i.v.* administration of  $[^{89}\text{Zr}]\text{Zr-DFO-}\alpha\text{CD133}$  (3.7-3.9 MBq, 10.0-10.5  $\mu\text{g}$ ) or  $[^{89}\text{Zr}]\text{Zr-DFO-hIgG}_1$  (3.3-3.5 MBq, 36-38  $\mu\text{g}$ ) to athymic nude mice ( $n = 4$  per cohort) bearing subcutaneous H82 xenografts. \*  $p < 0.05$ , \*\*\*  $p < 0.0001$  using 2-way ANOVA and Bonferroni adjustment. For the MIP images, min = 0%, max = 100%. (C) Representative maximum intensity projection PET/CT (left) and bioluminescence images (right) acquired 144 h after the *i.v.* administration of  $[^{89}\text{Zr}]\text{Zr-DFO-}\alpha\text{CD133}$  (3.7-3.9 MBq, 5-5.5  $\mu\text{g}$ ) to athymic nude mice ( $n = 4$ ) bearing orthotopic H82-*luc* xenografts in the parenchyma of the left lung. (D) White light images and autoradiographs of the left and right lungs of the mouse shown in panel C; the dotted lines in the autoradiographs represent the outline of the lung.

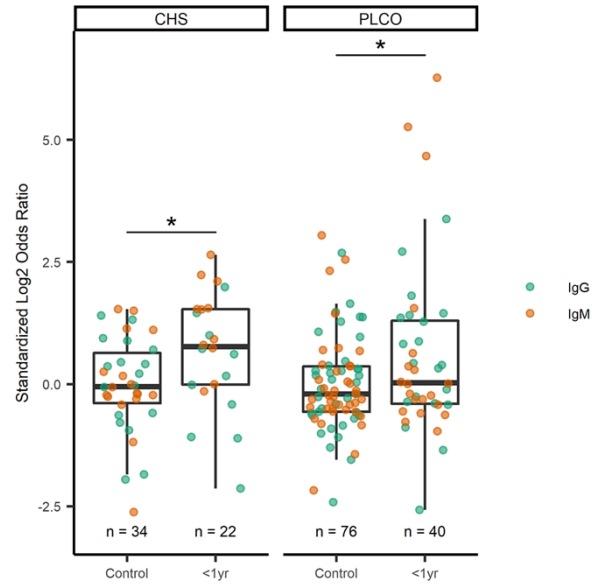


**FIGURE 6.** Expression of  $\alpha$ CD133 autoantibodies in the plasma of healthy controls or SCLC patients in two pre-diagnostic cohorts from the CHS and PLCO Screening Trial. \* $p < 0.05$  using 2-way ANOVA and Bonferroni adjustment.

## REFERENCES

1. Wang S, Zimmermann S, Parikh K, Mansfield AS, Adjei AA. Current diagnosis and management of small-cell lung cancer. *Mayo Clin Proc.* 2019;94:1599-1622.
2. Howlader N, Noone AM, Krapcho M, et al. SEER Cancer Statistics Review, 1975-2016. November 2019; based on November 2019 SEER data submission, posted to the SEER web site, April 2020. Accessed April 10, 2020.
3. The National Lung Screening Trial Research Team. Reduced lung-cancer mortality with low-dose computed tomographic screening. *N Engl J Med.* 2011;365:395-409.
4. Vant Westeinde SC, De Koning HJ, Thunnissen FB, et al. The role of the (18)F-fluorodeoxyglucose-positron emission tomography scan in the Netherlands Leuven Longkanker Screenings Onderzoek lung cancer screening trial. *J Thorac Oncol.* 2011;6:1704-1712.
5. Thomas A, Pattanayak P, Szabo E, Pinsky P. Characteristics and outcomes of small cell lung cancer detected by CT screening. *Chest.* 2018;154:1284-1290.
6. Glumac PM, Gallant JP, Shapovalova M, et al. Exploitation of CD133 for the targeted imaging of lethal prostate cancer. *Clinical Cancer Research.* 2020;26:1054-1064.
7. Qiu Z-x, Zhao S, Mo X-m, Li W-m. Overexpression of PROM1 (CD133) confers poor prognosis in non-small cell lung cancer. *International Journal of Clinical and Experimental Pathology.* 2015;8:6589-6595.
8. Wang X, Li B, Li R, et al. Anti-CD133 monoclonal antibody conjugated immunomagnetic nanosensor for molecular imaging of targeted cancer stem cells. *Sens Actuators B Chem.* 2018;255:3447-3457.
9. Yang K, Zhao Y, Du Y, Tang R. Evaluation of Hippo pathway and CD133 in radiation resistance in small-cell lung cancer. *J Oncol.* 2021;2021:1-8.
10. Kubo T, Takigawa N, Osawa M, et al. Subpopulation of small-cell lung cancer cells expressing CD133 and CD87 show resistance to chemotherapy. *Cancer Sci.* 2013;104:78-84.
11. Tsurumi C, Esser N, Firat E, et al. Non-invasive in vivo imaging of tumor-associated CD133/prominin. *PLoS One.* 2010;5:e15605.
12. Gaedicke S, Braun F, Prasad S, et al. Noninvasive positron emission tomography and fluorescence imaging of CD133+ tumor stem cells. *Proc Natl Acad Sci U S A.* 2014;111.
13. Liu Y, Yao X, Wang C, et al. Peptide-based <sup>68</sup>Ga-PET radiotracer for imaging CD133 expression in colorectal cancer. *Nucl Med Commun.* 2021:1144-1150.

14. George J, Lim JS, Jang SJ, et al. Comprehensive genomic profiles of small cell lung cancer. *Nature*. 2015;524:47-53.
15. Fung K, Vivier D, Keinänen O, Sarbisheh EK, Price EW, Zeglis BM. 89Zr-labeled AR20.5: A MUC1-targeting immunoPET probe. *Molecules*. 2020;25:1-13.
16. Rho JH, Lampe PD. High-throughput screening for native autoantigen-autoantibody complexes using antibody microarrays. *J Proteome Res*. 2013;12:2311-2320.
17. Hocking WG, Hu P, Oken MM, et al. Lung cancer screening in the randomized prostate, lung, colorectal, and ovarian (PLCO) cancer screening trial. *J Natl Cancer Inst*. 2010;102:722-731.
18. Rho JH, Ladd JJ, Li CI, et al. Protein and glycomic plasma markers for early detection of adenoma and colon cancer. *Gut*. 2018;67:473-484.
19. Mia-Jan K, Munkhdelger J, Lee MR, et al. Expression of CD133 in neuroendocrine neoplasms of the digestive tract: A detailed immunohistochemical analysis. *Tohoku J Exp Med*. 2013;229:301-309.
20. Rudin CM, Poirier JT, Byers LA, et al. Molecular subtypes of small cell lung cancer: a synthesis of human and mouse model data. *Nat Rev Cancer*. 2019;19:289-297.
21. Cui XY, Skretting G, Jing Y, Sun H, Sandset PM, Sun L. Hypoxia influences stem cell-like properties in multidrug resistant K562 leukemic cells. *Blood Cells Mol Dis*. 2013;51:177-184.
22. Gandhi L, Johnson BE. Paraneoplastic syndromes associated with small cell lung cancer. *J Natl Compr Canc Netw*. 2006;4:631-638.
23. Zaenker P, Gray ES, Ziman MR. Autoantibody production in cancer - The humoral immune response toward autologous antigens in cancer patients. *Autoimmun Rev*. 2016;15:477-483.
24. Johnson ML, Zvirbule Z, Laktionov K, et al. Rovalpituzumab tesirine as a maintenance therapy after first-line platinum-based chemotherapy in patients with extensive-stage-SCLC: Results from the phase 3 MERU study. *J Thorac Oncol*. 2021;16:1570-1581.
25. Krug LM, Milton DT, Jungbluth AA, et al. Targeting Lewis Y (Le<sup>y</sup>) in small cell lung cancer with a humanized monoclonal antibody, hu3S193: A pilot trial testing two dose levels. *J Thorac Oncol*. 2007;2:947-952.
26. Kwekkeboom DJ, Kam BL, Van Essen M, et al. Somatostatin receptor-based imaging and therapy of gastroenteropancreatic neuroendocrine tumors. *Endocr Relat Cancer*. 2010;17:53-73.

27. Zhou J, Chen J, Mokotoff M, Zhong R, Shultz LD, Ball ED. Bombesin/gastrin-releasing peptide receptor: A potential target for antibody-mediated therapy of small cell lung cancer. *Clin Cancer Res.* 2003;9:4953-4960.
28. Quaia E, Krug LM, Pandit-Taskar N, et al. The value of gamma camera and computed tomography data set coregistration to assess Lewis Y antigen targeting in small cell lung cancer by <sup>111</sup>Indium-labeled humanized monoclonal antibody 3S193. *Eur J Radiol.* 2008;67:292-299.
29. Jiang T, Collins BJ, Jin N, et al. Achaete-scute complex homologue 1 regulates tumor-initiating capacity in human small cell lung cancer. *Cancer Res.* 2009;69:845-854.
30. Huang YH, Klingbeil O, He XY, et al. POU2F3 is a master regulator of a tuft cell-like variant of small cell lung cancer. *Genes Dev.* 2018;32:915-928.
31. Lohrmann C, O'Reilly EM, O'Donoghue JA, et al. Retooling a blood-based biomarker: Phase I assessment of the high-affinity CA19-9 antibody HuMab-5B1 for immuno-PET imaging of pancreatic cancer. *Clin Cancer Res.* 2019;25:7014-7023.
32. Jansen MH, Lagerweij T, Sewing AC, et al. Bevacizumab targeting diffuse intrinsic pontine glioma: Results of 89Zr-bevacizumab PET imaging in brain tumor models. *Mol Cancer Ther.* 2016;15:2166-2174.
33. Koerner SP, André MC, Leibold JS, et al. An Fc-optimized CD133 antibody for induction of NK cell reactivity against myeloid leukemia. *Leukemia.* 2017;31:459-469.
34. Hu B, Zou Y, Zhang L, et al. Nucleofection with plasmid DNA for CRISPR/Cas9-mediated inactivation of programmed cell death protein 1 in CD133-specific CAR T cells. *Hum Gene Ther.* 2019;30:446-458.
35. Prasad S, Gaedicke S, Machein M, et al. Effective eradication of glioblastoma stem cells by local application of an AC133/CD133-specific T-cell-engaging antibody and CD8 T cells. *Cancer Res.* 2015;75:2166-2176.
36. Smith LM, Nesterova A, Ryan MC, et al. CD133/prominin-1 is a potential therapeutic target for antibody-drug conjugates in hepatocellular and gastric cancers. *Br J Cancer.* 2008;99:100-109.
37. Zhao L, Yang Y, Zhou P, et al. Targeting CD133 high colorectal cancer cells in vitro and in vivo with an asymmetric bispecific antibody. *J Immunother.* 2015;38:217-228.
38. Zhu X, Prasad S, Gaedicke S, Hettich M, Firat E, Niedermann G. Patient-derived glioblastoma stem cells are killed by CD133-specific CAR T cells but induce the T cell aging marker CD57. *Oncotarget.* 2015;6:171-184.

39. Wang Y, Chen M, Wu Z, et al. CD133-directed CAR T cells for advanced metastasis malignancies: A phase I trial. *Oncoimmunology*. 2018;7:1-13.
40. Feng KC, Guo Y-l, Liu Y, et al. Cocktail treatment with EGFR-specific and CD133-specific chimeric antigen receptor-modified T cells in a patient with advanced cholangiocarcinoma. *J Hematol Oncol*. 2017;10:1-11.
41. Dai H, Tong C, Shi D, et al. Efficacy and biomarker analysis of CD133-directed CAR T cells in advanced hepatocellular carcinoma: a single-arm, open-label, phase II trial. *Oncoimmunology*. 2020;9:1-8.

## *Supplemental Information*

### **Contents**

Supplemental Methods .....	2
Supplemental Figures .....	9
Supplemental Tables.....	22

## SUPPLEMENTAL METHODS

### Cell culture

The human SCLC cell lines NCI-H82 (“H82”), NCI-H69 (“H69”), and K562 were purchased from the American Type Culture Collection (ATCC) in 2020 and periodically authenticated by the Specimen Processing/Research Cell Bank Shared Resource using Short Tandem Repeat (STR) Combined DNA Index System typing. Cells were maintained in either DMEM or RPMI-1640 Medium supplemented with 10% heat-inactivated fetal calf serum, 100 units/mL penicillin, 100 units/mL streptomycin, 2 mM L-glutamine, 10 mM HEPES, 4.5 g/L D-glucose, 1.5 g/L sodium bicarbonate, and 1 mM sodium pyruvate in an incubator at 37°C and 5% CO<sub>2</sub>. Cells were passaged upon reaching 80% confluency. The H82 cells tend to form large aggregates in suspension, so the aggregates were dissociated by incubating the cells with Gibco™ TrypLE™ Express Enzyme (1×) with phenol red (ThermoFisher) for 5 minutes between each passage. The cells were also strained using cell strainers (MACS SmartStrainers, 30 µm and 70 µm, Miltenyi Biotec; Auburn, CA, USA) to ensure a homogenous cell suspension mixture prior to any experiments or xenografting. Anti(α)-CD133 monoclonal antibody was Protein A purified from spent Hybridoma-SFM media (#12045, Gibco; Grand Island, NY) used to grow hybridoma Clone HB #7 (Developmental Studies Hybridoma Bank; Iowa City, IA).

### Production and culture of H82-luc cells

H82 cells were directly transfected with 2 µg of pcDNA3.1(+)/Luc2=tdT plasmid (Addgene #32904) using Nucleofector Kit L (Lonza VVCA-1005) and program A-020. Transfected cells were selected for 7 days using 1000 µg/mL G418 (Invitrogen) and subsequently FACS sorted for Tomato red fluorescent protein positive cells to >95% purity. The H82-luc cells were cultured and maintained as described above.

### Animals

Six to eight-week-old female athymic nude mice (Jackson Laboratory #007850 or #002019) were allowed to acclimatize approximately 1 week prior to inoculation. Animals were housed in ventilated cages and given food and water *ad libitum*. NIRF imaging mice were placed on an alfalfa-free diet at the time of tumor cell inoculation to limit autofluorescence. All animal work

was approved of by the respective IACUCs of Memorial Sloan Kettering Cancer Center and Fred Hutchinson Cancer Research Center.

### Mouse xenograft models

Mice were anesthetized by inhalation of 2% isoflurane (Baxter Healthcare; Deerfield, IL)/oxygen gas mixture. For subcutaneous tumors, the injection site was sanitized with an ethanol wipe and  $3\text{-}5 \times 10^6$  H82 cells (150-200  $\mu\text{L}$ ) in media or Hanks Balanced salt solution — with or without 1:1 Matrigel (Corning Life Sciences; Corning, NY) — were injected subcutaneously in the flank. For orthotopic tumors, an incision was made under the left scapula and  $2\text{-}5 \times 10^6$  H82 or H82-*luc* cells (40  $\mu\text{L}$ ) were injected into the parenchyma of the left lung. To ensure homogenous tumors, the cell suspension was mixed thoroughly prior to each inoculation. The H82 and H82-*luc* tumors reached an acceptable size for imaging and biodistribution studies ( $\sim 50\text{-}100 \text{ mm}^3$ ) after 2-4 weeks.

### MR and NIRF imaging

All imaging was performed with mice under anesthesia with a 2% isoflurane/oxygen gas mixture. MRI was performed on a 1.0T ICON system (Bruker BioSpin; San Jose, CA) running ParaVision 6.0.1. SinglePulse and Localizer scans were acquired followed by primary imaging using T1 FLASH sequence (15, 1 mm slices, scan time 3-5 minutes). Animals were respiratory gated using an ERT control/gating module (Small Animal Instruments; Stoney Brook, NY) and PC-SAM32. Image reconstruction was done with Osirix Lite (v11.03, Bernex, Switzerland).

NIRF was performed using  $\alpha\text{CD133}$  mAb (HB #7, Developmental Studies Hybridoma Bank, Iowa City, IA) conjugated to the near-infrared fluorophore CF770 (#92222, Biotium; Fremont, CA) according to the manufacturer's instructions. Mice bearing subcutaneous or orthotopic H82 flank tumors were injected retro-orbitally with  $\alpha\text{CD133}\text{-CF770}$  (50  $\mu\text{g}$ )  $\sim 3\text{-}4$  weeks after cell inoculation. NIRF was performed up to 4 days after  $\alpha\text{CD133}\text{-CF770}$  injection using an IVIS Spectrum (Em/Ex: 745/780, small bin, f-stop 4, Stage B) with Living Image v4.7.2 (Perkin Elmer). Lungs were excised after terminal *in vivo* imaging and re-imaged *ex vivo* with the aforementioned settings.

### PET imaging of mice bearing subcutaneous xenografts

Images were obtained using a microPET Focus 120 small animal imaging system (Siemens Medical Solutions; Malvern, PA). Mice (n = 4 per group) underwent static scans between 24 and 144 h after the intravenous tail vein administration of either [<sup>89</sup>Zr]Zr-DFO- $\alpha$ CD133 [3.7 -3.9 MBq (100-105  $\mu$ Ci), 10-10.5  $\mu$ g, in 100  $\mu$ L of PBS] or [<sup>89</sup>Zr]Zr-DFO-hIgG<sub>1</sub> [3.3-3.5 MBq (90-95  $\mu$ Ci), 36-38  $\mu$ g, in 100  $\mu$ L of PBS] for a total scan time of 10-30 minutes. The counting rates in the reconstructed images were converted to activity concentrations (percentage injected dose per gram of tissue [%ID/g]) using a system calibration factor derived from the imaging of a mouse-sized water-equivalent phantom containing <sup>89</sup>Zr. Maximum intensity projection (MIP) images were generated from 3-dimensional ordered subset expectation maximization reconstruction (3D-OSEM). The resulting images were processed using ASIPro VM<sup>TM</sup>. Region-of-interest analysis was performed using Amide Medical Imaging software. Ellipsoid regions-of-interest were drawn around the heart (for blood), liver, and tumor for each mouse using the images acquired at 24, 72, 120, and 144 h post-injection. Mean %ID/g values were used for both liver and blood; max values were used for the tumor.

#### PET imaging of mice bearing orthotopic xenografts

Images were obtained using a Inveon PET/CT small animal imaging system (Siemens Medical Solutions; Malvern, PA). Mice (n = 4) underwent static scans between 24 and 144 h after the intravenous tail vein administration of [<sup>89</sup>Zr]Zr-DFO- $\alpha$ CD133 [3.7 -3.9 MBq (100-105  $\mu$ Ci), 5-5.5  $\mu$ g, in 100  $\mu$ L of PBS] for a total scan time of 10-30 minutes. The counting rates in the reconstructed images were converted to activity concentrations (percentage injected dose per gram of tissue [%ID/g]) using a system calibration factor derived from the imaging of a mouse-sized water-equivalent phantom containing <sup>89</sup>Zr. Maximum intensity projection (MIP) images were generated from 3-dimensional ordered subset expectation maximization reconstruction (3D-OSEM). The resulting images were processed using Amide Medical Imaging software.

#### Bioluminescence imaging

To monitor the growth of the orthotopically implanted H82-*luc* cells, bioluminescence images of the mice were collected using an IVIS Spectrum-CT instrument. To this end, 100  $\mu$ L of 30 mg/mL firefly D-luciferin in PBS was injected into the mouse *i.p.*. Subsequently, the mice were

anesthetized with 2% isoflurane/O<sub>2</sub>. At 15 minutes post-injection, the mice were imaged in the prone and lateral positions; all images were analyzed with Living Image software.

### Instrumentation

All instruments were calibrated and maintained according to standard quality control practices and procedures. UV-Vis measurements were taken on a Shimadzu BioSpecNano Micro-volume UV-Vis Spectrophotometer (Shimadzu Scientific Instruments; Kyoto, Japan). Radioactivity measurements were taken using a CRC-15R Dose Calibrator (Capintec, Inc; Ramsey, NJ) and Automatic Wizard<sup>2</sup> gamma counter (PerkinElmer; Waltham, MA).

### Synthesis of DFO- $\alpha$ CD133

$\alpha$ CD133 (1.0 mg) in Chelex 100-treated (Bio-Rad Laboratories; Hercules, CA) phosphate-buffered saline (Chelex PBS, pH 7.4) was diluted to a final concentration of 1.0 mg/mL. The pH of the solution was adjusted to 8.8-9.0 with 0.1 M Na<sub>2</sub>CO<sub>3</sub>, 35 equivalents of *p*-SCN-Bn-DFO (7.05  $\mu$ L, 25 mg/mL in DMSO) were added in small aliquots, and the resulting solution was incubated on a thermomixer (37°C, 500 rpm, 1h). The immunoconjugate was purified using size exclusion chromatography (PD-10 column; GE Healthcare; Chicago, IL), eluted with 2 mL of Chelex PBS, and concentrated using 2 mL Amicon Ultra centrifugal filters with a 50 kDa molecular weight cut-off (MilliporeSigma). An isotype control immunoconjugate, DFO-hIgG<sub>1</sub>, was prepared in an analogous manner using 1 mg of mAb and 20 equivalents of *p*-SCN-Bn-DFO (4.02  $\mu$ L, 25 mg/mL in DMSO). See *Supplemental Figure 5* for a schematic of the bioconjugation reaction.

### Degree of labeling determination

Matrix-assisted laser desorption/ionization (MALDI) mass spectrometry was used to determine the number of DFO moieties per antibody (Alberta Proteomics and Mass Spectrometry Facility, University of Alberta, Canada). The immunoconjugate was analyzed in triplicate using a Bruker Ultraflex MALDI-ToF/ToF (Bruker Daltonik GmbH, Bremen, Germany). To wit, 1  $\mu$ L of each sample (1 mg/mL in water) was mixed with 1  $\mu$ L of sinapic acid (10 mg/mL in 50% acetonitrile/water and 0.1% trifluoroacetic acid). 1  $\mu$ L of the sample/matrix solution was then spotted onto a stainless-steel target plate and allowed to air dry. Ions were analyzed in positive

mode, and external calibration was performed using a standard protein mixture of bovine serum albumin. The difference between the mass of each DFO-bearing immunoconjugate and its unmodified parent antibody was calculated, and the degree of labeling was determined via division by the mass of *p*-SCN-Bn-DFO (752.9 Da).

### Radiolabeling

DFO- $\alpha$ CD133 (0.1 mg) was diluted in Chelex PBS to a final concentration of 0.5 mg/mL. [ $^{89}\text{Zr}$ ]Zr $^{4+}$  [9.25 MBq – 37 MBq (250  $\mu\text{Ci}$  – 1000  $\mu\text{Ci}$ )] in 1.0 M oxalic acid was diluted with Chelex PBS and the solution pH was adjusted to 7.0-7.5 with 1.0 M Na $_2$ CO $_3$  (final volume 100  $\mu\text{L}$ ). After CO $_2$  bubbling ceased, the  $^{89}\text{Zr}$  solution was added to the antibody solution, mixed thoroughly, and reacted on a thermomixer (500 rpm, 37  $^\circ\text{C}$ , 15 min). The reaction progress was assayed using glass-fiber, silica-impregnated instant thin-layer chromatography (iTLC) paper (Pall Corp.; East Hills, NY), eluted with EDTA eluent (50 mM, pH 5.0), and analyzed on an AR-2000 radio-TLC plate reader using Winscan Radio-TLC software (Bioscan, Inc.; Washington, DC). Following completion of the reaction, any free [ $^{89}\text{Zr}$ ]Zr $^{4+}$  was removed from the radioimmunoconjugate solution using size exclusion chromatography. The radiochemical purity of the final radiolabeled construct was assayed using radio-iTLC with EDTA as the eluent (50 mM, pH 5.0). For the radiosynthesis of [ $^{89}\text{Zr}$ ]Zr-DFO-hIgG $_1$ , the same parameters were used. All radiolabeling studies were performed in triplicate.

### Radioimmunoconjugate stability assays

The stability of the radioimmunoconjugate was investigated by incubating [ $^{89}\text{Zr}$ ]Zr-DFO- $\alpha$ CD133 in human serum on a thermomixer at 500 rpm and 37  $^\circ\text{C}$  for 5 days. Every 24 h, the radiochemical purity of [ $^{89}\text{Zr}$ ]Zr-DFO- $\alpha$ CD133 was determined in triplicate via radio-TLC with an eluent of 50 mM EDTA (pH 5.0).

### Immunoreactivity assays

The immunoreactivity of [ $^{89}\text{Zr}$ ]Zr-DFO- $\alpha$ CD133 was determined using a cell-saturation study. Briefly,  $15 \times 10^6$  H82 or K562 cells were washed 3 $\times$  with ice-cold media, centrifuged (600g, 2 min), and the supernatant discarded. Ice-cold media (200  $\mu\text{L}$ ) with 1  $\mu\text{L}$  of [ $^{89}\text{Zr}$ ]Zr-DFO- $\alpha$ CD133 (1  $\mu\text{g}/\text{mL}$  in 1% BSA-PBS) was added to the cell pellet, mixed thoroughly, and allowed

to incubate for 1 h. After the incubation period, the cells were centrifuged, and the supernatant was reserved. The cells were washed 2× with ice-cold media and the supernatants were each reserved in a separate microcentrifuge tube. The samples were then measured on an  $^{89}\text{Zr}$ -calibrated gamma counter, with the activities (counts/minute) background and decay corrected to the start of the run. The immunoreactivity was expressed as a percentage by comparing the activity remaining in the cells to the total activity (cells + supernatant + washes). For the blocking experiments, the assay was run identically, but 5  $\mu\text{g}$  of unlabeled  $\alpha\text{CD133}$  were co-incubated with the cells along with the [ $^{89}\text{Zr}$ ]Zr-DFO- $\alpha\text{CD133}$ .

### Biodistribution studies

Following terminal PET imaging (144 h post-injection), the mice were euthanized via  $\text{CO}_2$  asphyxiation followed by cervical dislocation. The 15 most relevant organs were collected, rinsed in water, dried, weighed, and quantified using an  $^{89}\text{Zr}$ -calibrated Automatic Wizard<sup>2</sup>  $\gamma$ -counter (PerkinElmer). The counts/minute in each tissue was background and decay corrected to the start of the activity measurement. The %ID/g for each sample was calculated by normalization to the total injected activity.

### Autoradiography

Following the final PET timepoint, the mice were sacrificed via  $\text{CO}_2$  asphyxiation. The lungs were perfused through the right ventricle of the heart with 3 mL PBS using a 28 gauge needle, and the lungs were inflated with roughly 2 mL of a 50/50 formalin/OCT mixture inserted into the trachea with a 23 gauge needle. The inflated lungs were immediately submerged in formalin and allowed to incubate for 24 hours. After 24 hours, the lungs were washed with 20% sucrose overnight and the right and left lungs were separated. The left lungs and the inferior lobe of the right lungs were then embedded in a cryomold with OCT and immediately frozen. 10  $\mu\text{m}$  slices of the tissue were cut using a cryostat microtome and collected onto slides. The slides were then placed into a cassette with a clean phosphor imager plate (FujiFilm Imaging Plate, BAS-MS) and the cassette was stored in the dark for 48 hours. Following this, the radioactivity on the phosphor imager plate was scanned using Typhoon FLA 7000 instrumentation.

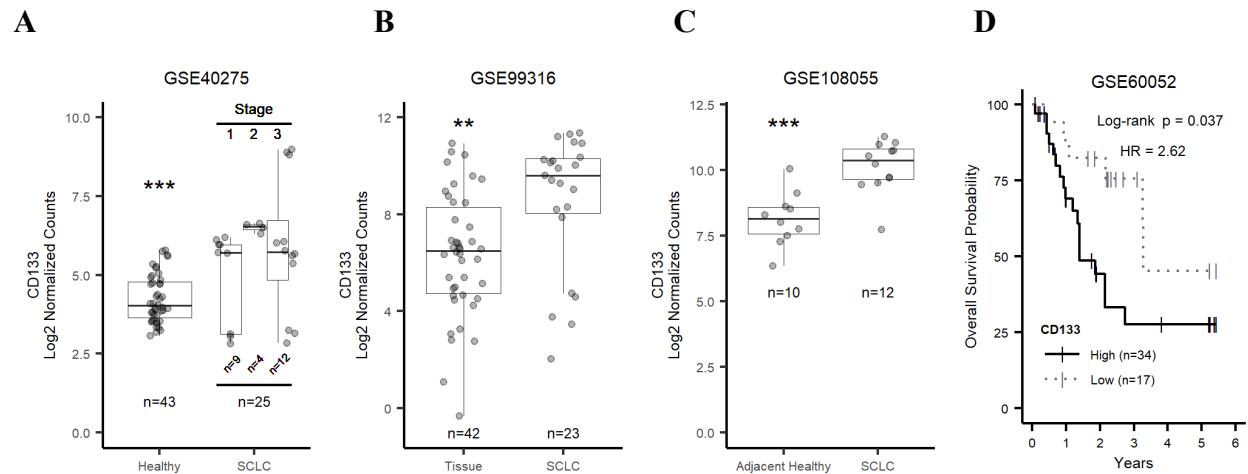
### Statistics and graphing

Figures and statistics were prepared using RStudio (v1.4.1717). Where appropriate, t-tests or ANOVA with post-hoc analyses were performed using the `rstatix` (v0.70) and `emmeans` (v1.6.2.1) packages. Plots and tables were generated using the `ggplot2` (v3.3.5), `ComplexHeatmap` (v2.8.0), `ggpubr` (v0.4.0), and `gt` (v0.3.0) packages.

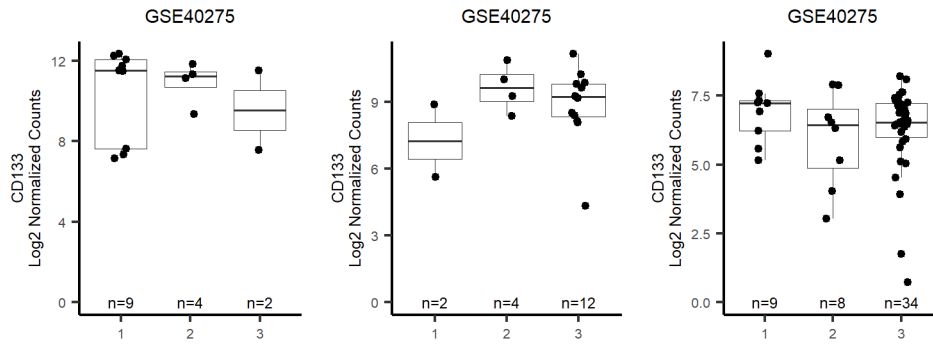
### Data availability

RNA Sequencing (RNAseq) data from 289 series were procured from the Gene Expression Omnibus (GEO) by searching for “small cell lung cancer” or “SCLC”. Further filtering by organism (*Homo sapiens*), assay type (Expression profiling by array), sample type (tissue from healthy, SCLC, or other lung cancer patients, but not cell lines only), and at least 10 SCLC cases resulted in 6 cohorts: [GSE99316](#), [GSE40275](#), [GSE29066](#), [GSE108055](#), [GSE149507](#), and [GSE60052](#) whose characteristics are outlined in Tables S1 and S2. Whole genome sequencing was used to assess expression data and somatic mutations from the Cancer Cell Line Encyclopedia (CCLE) using the [DepMap Public 21Q3](#) dataset or SCLC patient samples as described by George *et al.* in their Supplementary Table 3 (reference #14 from the main text).

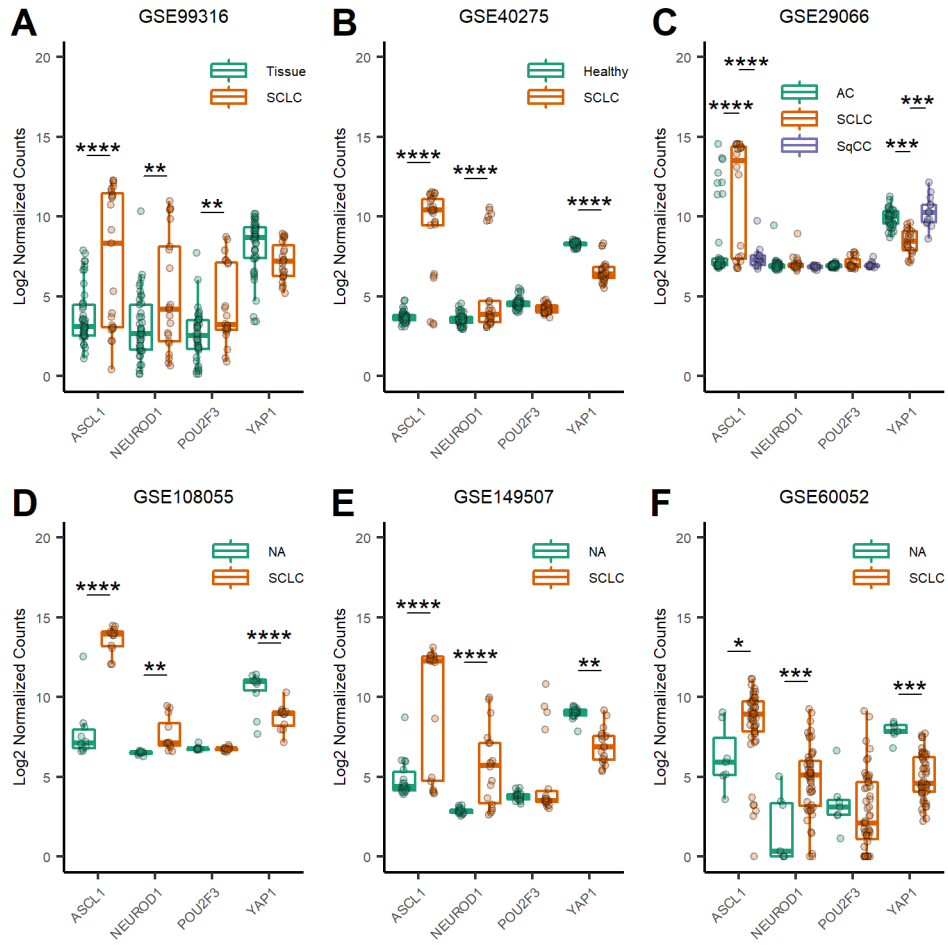
## SUPPLEMENTAL FIGURES



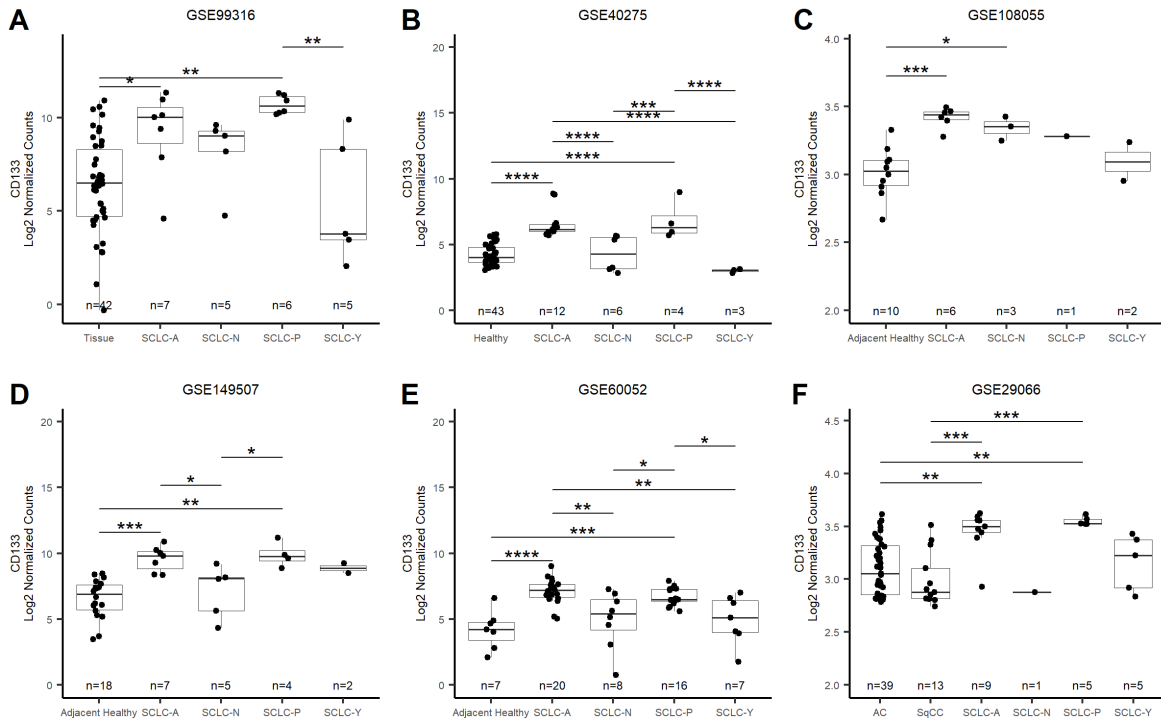
**SUPPLEMENTAL FIGURE 1.** CD133 mRNA expression in publicly available datasets from the Gene Expression Omnibus (GEO). A) A comparison of CD133 mRNA in healthy lung tissue vs SCLC tumor tissue by stage from commercially purchased RNA (GSE40275) (stats comparing healthy vs all SCLC). B) Levels of CD133 transcripts in commercially procured RNA from healthy tissues vs SCLC tumors from Japanese patients (GSE99316). C) CD133 mRNA levels in adjacent healthy SCLC tumor tissue from patients in the USA. D) Kaplan-Maier survival curve for mean-stratified (6.34 mean log<sub>2</sub> expression cut-point) SCLC patients with low-vs-high CD133 mRNA expression (HR=hazard ratio) \*\* p < 0.01, \*\*\* p < 0.001 by t-test or one-way ANOVA with Tukey adjustment.



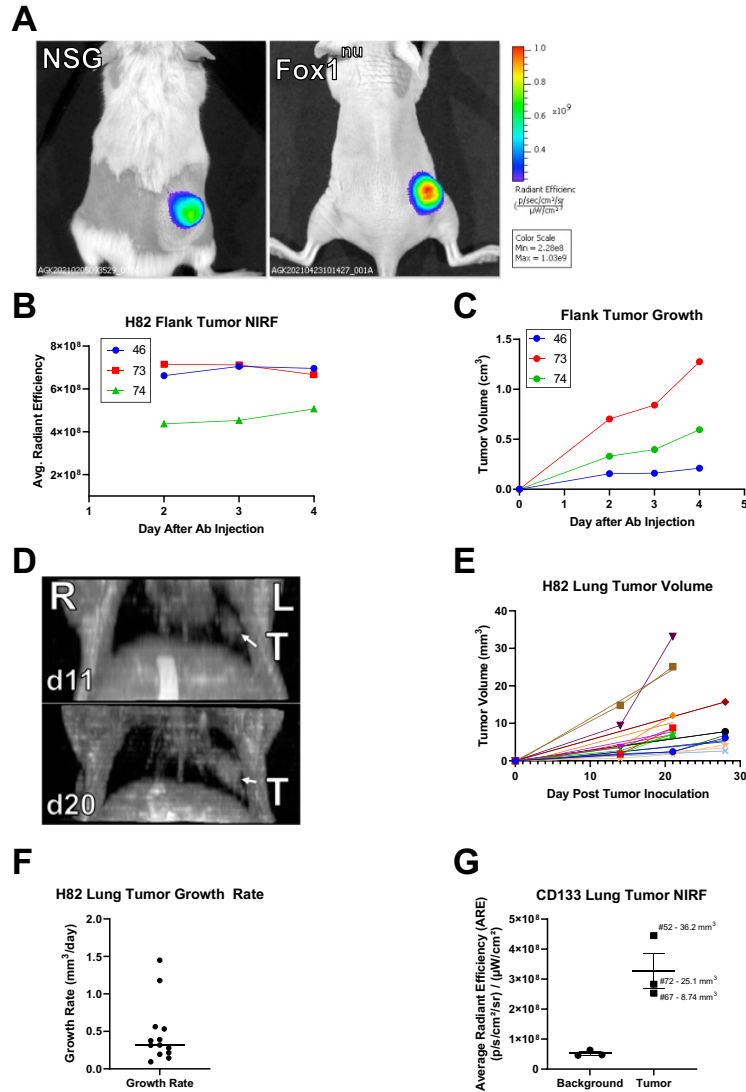
**SUPPLEMENTAL FIGURE 2.** CD133 expression by SCLC Stage. RNAseq expression of CD133 by stage in SCLC GEO data sets. No significant differences were detected by ANOVA.



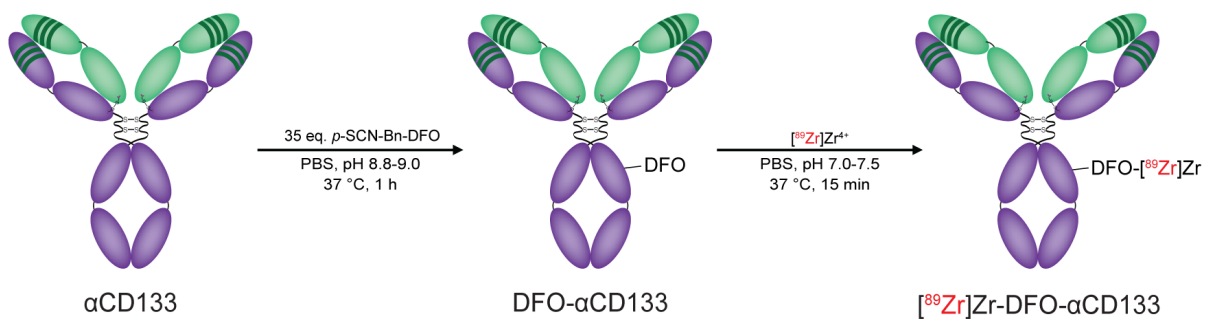
**SUPPLEMENTAL FIGURE 3.** Relative expression of each subtype marker in SCLC GEO data sets. AC = adenocarcinoma, SCLC = small cell lung cancer, SqCC = squamous cell carcinoma, NA = normal adjacent. Two-way ANOVA with Bonferroni multiplicity-adjusted post-hoc pairwise comparisons \*  $p < 0.05$ , \*\*  $p < 0.01$ , \*\*\*  $p < 0.001$ , \*\*\*\*  $p < 0.0001$ .



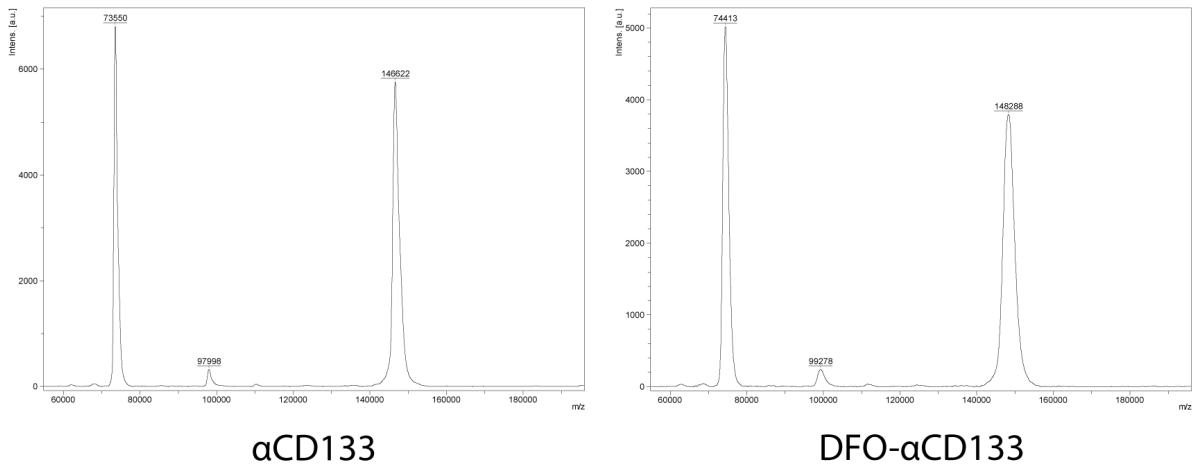
**SUPPLEMENTAL FIGURE 4.** CD133 expression by SCLC subtype. CD133 expression was compared between SCLC and A) normal tissue, B) healthy patients, C-E) adjacent normal tissue, and F) NSCLC as a function of SCLC subtype. \*  $p < 0.05$ , \*\*  $p < 0.01$ , \*\*\*  $p < 0.001$ , \*\*\*\*  $p < 0.0001$  by t-test or one-way ANOVA for overall effect (not by subtype)



**SUPPLEMENTAL FIGURE 5.**  $\alpha$ CD133-CF770 NIRF imaging of H82 xenografts. A) H82 SCLC cells can form tumors in two mouse strains with varying degrees of immunity and are detectable via NIRF imaging with  $\alpha$ CD133-CF770. NOD scid gamma (NSG) mice lack mature B cells, T cells natural killer cells, and complement, and have defective dendritic cells and macrophages. Fox1<sup>nu</sup> nude mice lack mature T cells and have partially defective B cells. B) CD133 NIRF signal from mice with flank H82 tumors did not vary over imaging days. C) Growth of H82 flank tumor during experiment. D) Coronal MRI of H82 tumor in the left lung (arrow) at 11 and 20 days after cell inoculation. E) H82 lung tumor volume and F) growth rate over duration of experiment. F) NIRF signal of H82 lung tumor compared to background (foot) at 4 days after antibody injection. Animal number and tumor volume are as labeled.

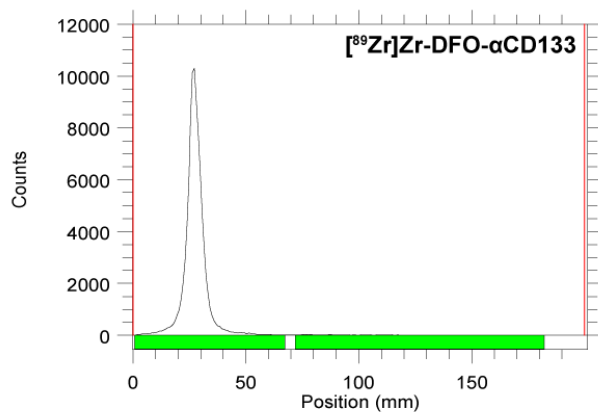
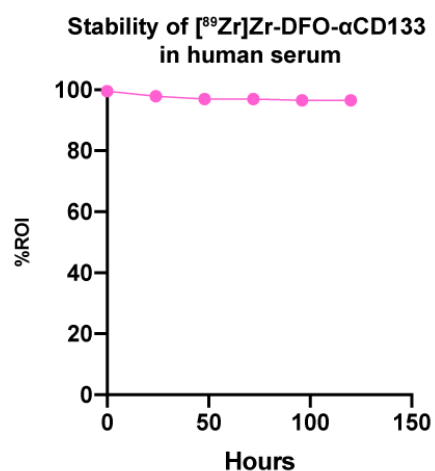


**SUPPLEMENTAL FIGURE 6.** Schematic of the bioconjugation and radiolabeling of  $\alpha\text{CD133}$ .

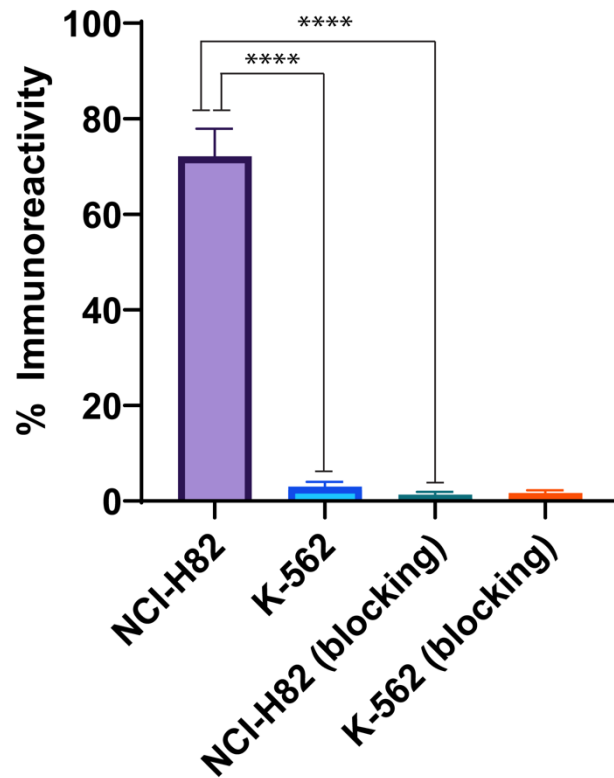
**A.****B.**

Sample	Average Mass (Da) n = 3	DOL (DFO/mAb)
$\alpha$ CD133	146827.17 $\pm$ 282.82	-
DFO- $\alpha$ CD133	148514.17 $\pm$ 326.24	2.22 $\pm$ 0.41

**SUPPLEMENTAL FIGURE 7.** A) Representative MALDI-ToF mass spectrograms used to determine the degree of labeling of DFO- $\alpha$ CD133; B) Data used to determine the degree of labeling of DFO- $\alpha$ CD133.

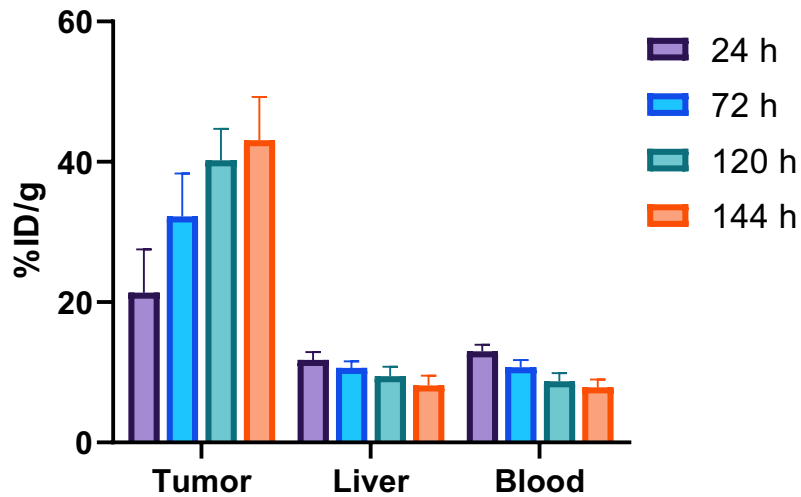
**A.****B.**

**SUPPLEMENTAL FIGURE 8.** The characterization of  $[^{89}\text{Zr}]\text{Zr-DFO-}\alpha\text{CD133}$ . A) iTLC of purified  $[^{89}\text{Zr}]\text{Zr-DFO-}\alpha\text{CD133}$  indicating >99% radiochemical purity; B) stability assay of  $[^{89}\text{Zr}]\text{Zr-DFO-}\alpha\text{CD133}$  in human serum.

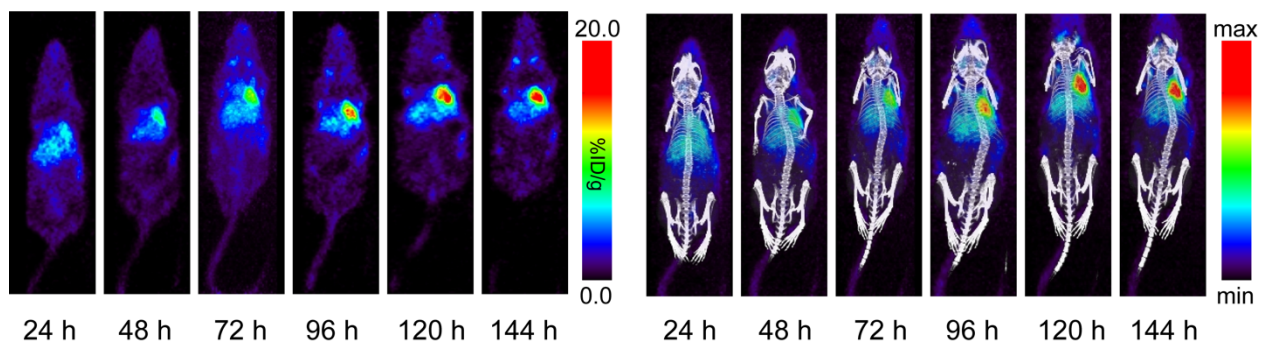


**SUPPLEMENTAL FIGURE 9.** Immunoreactivity assay for [<sup>89</sup>Zr]Zr-DFO- $\alpha$ CD133 in which the radioimmunoconjugate (1 ng) was incubated with CD133-positive NCI-H82 cells and CD133-negative K562 cells ( $1.5 \times 10^7$ ). For the blocking experiments, 5  $\mu$ g of unlabeled  $\alpha$ CD133 was co-incubated with the cells along with [<sup>89</sup>Zr]Zr-DFO- $\alpha$ CD133. \*\*\*\* =  $p < 0.0001$  via an unpaired t-test; statistical significance was determined using GraphPad Prism 8.3.0 software.

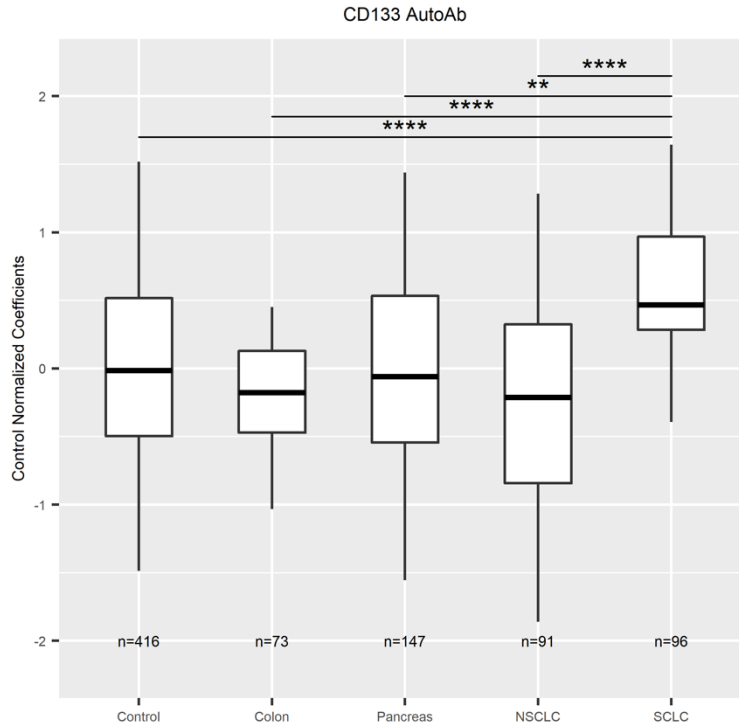
## PET ROI Quantification



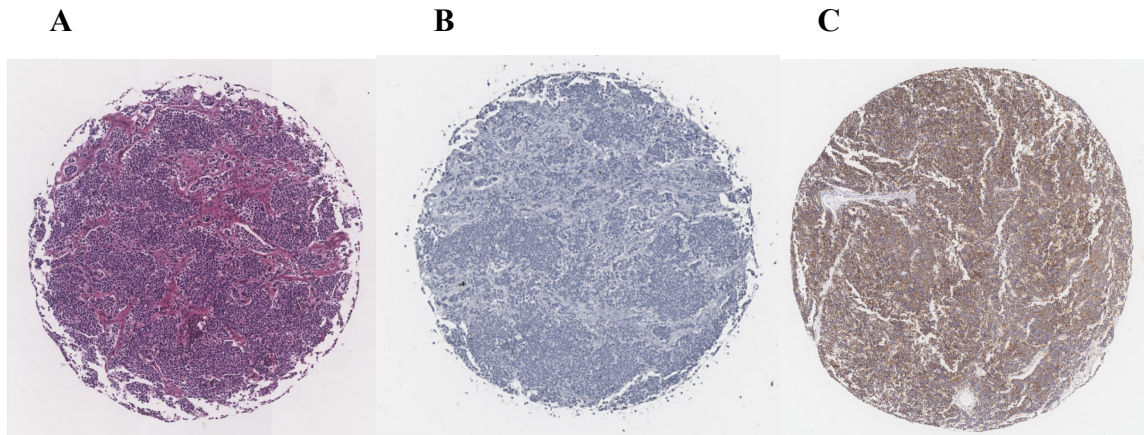
**SUPPLEMENTAL FIGURE 10.** Region-of-interest quantification of the activity concentrations in the tumor, liver, and blood obtained from PET images acquired 24, 72, 120, and 144 h after the intravenous administration of [ $^{89}\text{Zr}$ ]Zr-DFO- $\alpha$ CD133 [3.7 -3.9 MBq, 10-10.5  $\mu\text{g}$ , in 100  $\mu\text{L}$  of PBS] to athymic nude mice bearing subcutaneous H82 xenografts ( $n = 4$  per cohort). Mean %ID/g values  $\pm$  standard deviation were used for both the liver and blood; max %ID/g values  $\pm$  standard deviation were used for the tumor.



**SUPPLEMENTAL FIGURE 11.** Representative coronal slice PET (left) and maximum intensity projection PET/CT (right) images acquired 24, 72, 120, and 144 h after the *i.v.* administration of [<sup>89</sup>Zr]Zr-DFO- $\alpha$ CD133 (3.7-3.9 MBq, 5-5.5  $\mu$ g) to athymic nude mice (n = 4) bearing orthotopic H82-*luc* xenografts.



**SUPPLEMENTAL FIGURE 12.** Levels of  $\alpha$ CD133 autoantibodies from patient plasma across various cancer types quantified using antibody microarrays. Coefficients were mean-centered to controls within each experiment, controls were combined and compared to tumors. Boxes = interquartile range, whiskers = 1x interquartile range above boxes. Bar = mean. NSCLC = non-small cell lung cancer. \*\*  $p < 0.01$ , \*\*\*\*  $p < 0.0001$  by t-test or one-way ANOVA with Tukey adjustment.



**SUPPLEMENTAL FIGURE 13.** Human IgG is not detected in SCLC tumors. A small cell lung cancer tumor microarray containing 45 SCLC cases in duplicate (90 cores total) were stained for A) H&E or B) human IgG (none of the 90 cores shows significant staining), or C) a CD133=positive SCLC core from the data in Figure 2.

## SUPPLEMENTAL TABLES

SUPPLEMENTARY TABLE 1. GEO RNAseq Data Set Characteristics						
Accession	Manufacturer	Array	Tissue			Country
			Normal	SCLC	AC/SCC	
<a href="#">GSE99316</a>	Affymetrix	Human Genome U133 Plus 2.0 Array	23	43	3	Japan/Commercial
<a href="#">GSE40275</a>	Affymetrix	Human Exon 1.0 ST Array	43	25		Commercial
<a href="#">GSE29066</a>	Illumina	HumanHT-12 v3.0 Expression BeadChip	20	39	13	Sweden
<a href="#">GSE108055</a>	Illumina	HumanWG-6 v2.0 Expression BeadChip	10 <sup>1</sup>	12		USA
<a href="#">GSE149507</a>	Affymetrix	Human Genome U133 Plus 2.0 Array	18 <sup>1</sup>	18		China
<a href="#">GSE60052</a>	Illumina	HiSeq 2000 (Homo Sapiens)	7 <sup>1</sup>	51		China
<sup>1</sup> Adjacent healthy tissue, not necessarily paired						
Normal, normal lung; SCLC, small cell lung cancer; AC, adenocarcinoma; SCC, squamous cell carcinoma						

**SUPPLEMENTARY TABLE 2. GEO RNAseq data patient characteristics**

	GEO Data Set					
	GSE99316	GSE40275	GSE29066	GSE108055	GSE149507	GSE60052
<b>Sex</b>						
Male		48 (57.1%)	31 (43%)	6 (50%)	26 (27.2%)	45 (90%)
Female		36 (42.9%)	41 (57%)	6 (50%)	10 (27.8%)	5 (10%)
<b>Age (years)</b>						
Mean		66	66.4		57	57.8
Range		38 – 80	36 – 85		37 – 71	36 – 78.3
<b>Smoker</b>						
Ever			10 (39%)	11 (91.7%)	24 (66.7%)	35 (70%)
No			56 (77.8%)			15 (30%)
Never				1 (8.3%)	6 (16.7%)	
<b>Smoker</b>						
Unknown			6 (8.3%)		6 (16.7%)	
<b>Stage</b>						
I				3 (25%)		
IA		5 (12.2%)	18 (25%)			6 (12%)
IB		15 (36.6%)	27 (37.5%)			2 (4%)
II				3 (25%)		
IIA		4 (9.8%)	8 (11.1%)		4 (11.1%)	4 (8%)
IIB		3 (7.3%)	7 (9.7%)		8 (22.2%)	4 (8%)
III				4 (33.3%)		
IIIA		8 (19.5%)	6 (8.3%)		10 (27.8%)	28 (56%)
IIIB		6 (14.6%)			14 (38.9%)	5 (10%)
IV				2 (16.7%)		1 (2%)
Unknown			6 (8.3%)			
<b>Neoadjuvant Therapy</b>						
Treated					6 (16.7%)	8 (16%)
Naïve					24 (66.7%)	42 (84%)
Unknown					6 (16.7%)	

<b>SUPPLEMENTARY TABLE 3. CHS and PLCO patient characteristics</b>				
	<b>CHS</b>		<b>PLCO</b>	
	<b>Control</b>	<b>&lt;1 Year</b>	<b>Control</b>	<b>&lt;1 Year</b>
<b>Time to Dx</b>				
<b>Days</b>	—	195 (19 – 328)	—	344 (18 – 364)
<b>Sex</b>				
<b>Male</b>	14 (41.2%)	8 (36.4%)	50 (65.8%)	24 (60%)
<b>Age (years)</b>				
<b>≤ 59</b>			18 (23.7%)	14 (35%)
<b>60-64</b>			26 (34.2%)	8 (20%)
<b>65-69</b>	14 (41.2%)	10 (45.5%)	26 (34.2%)	14 (35%)
<b>≥ 70</b>	20 (58.8%)	12 (54.5%)	6 (7.9%)	4 (10%)
<b>Smoker</b>				
<b>Current</b>	12 (35.3%)	8 (36.4%)	48 (63.2%)	26 (65%)
<b>Former</b>	22 (64.7%)	14 (63.6%)	24 (31.6%)	12 (30%)
<b>Never</b>			4 (5.3%)	2 (5%)

<b>PET ROI Quantification (%ID/g)</b>				
<b>Organ</b>	<b>24 h</b>	<b>72 h</b>	<b>120 h</b>	<b>196 h</b>
<b>Tumor</b>	21.3 ± 6.2	32.2 ± 6.1	40.2 ± 4.5	43.1 ± 6.2
<b>Liver</b>	11.7 ± 1.2	10.6 ± 0.9	9.4 ± 1.4	8.1 ± 1.4
<b>Blood</b>	13.0 ± 0.9	10.7 ± 1.1	8.7 ± 1.2	7.8 ± 1.1

**SUPPLEMENTAL TABLE 4.** Region-of-interest quantification of the activity concentrations in the tumor, liver, and blood obtained from PET images acquired 24, 72, 120, and 144 h after the intravenous administration of [<sup>89</sup>Zr]Zr-DFO- $\alpha$ CD133 [3.7 -3.9 MBq, 5-5.5  $\mu$ g, in 100  $\mu$ L of PBS] to athymic nude mice bearing subcutaneous H82 xenografts (n = 4). Mean %ID/g values  $\pm$  standard deviation were used for both the liver and blood; max %ID/g values  $\pm$  standard deviation were used for the tumor.

<b>%ID/g (percentage of injected dose per gram of organ)</b>		
<b>Organ</b>	<b>[<sup>89</sup>Zr]Zr-DFO-<math>\alpha</math>CD133</b>	<b>[<sup>89</sup>Zr]Zr-hIgG1</b>
<b>Blood</b>	10.1 $\pm$ 1.9	10.0 $\pm$ 2.2
<b>Tumor</b>	50.8 $\pm$ 7.7	5.8 $\pm$ 4.0
<b>Heart</b>	2.4 $\pm$ 1.0	2.3 $\pm$ 0.8
<b>Lungs</b>	3.7 $\pm$ 2.3	3.4 $\pm$ 2.7
<b>Liver</b>	4.8 $\pm$ 2.4	2.9 $\pm$ 0.7
<b>Spleen</b>	4.5 $\pm$ 2.1	3.4 $\pm$ 2.3
<b>Pancreas</b>	0.6 $\pm$ 0.1	0.6 $\pm$ 0.5
<b>Stomach</b>	0.5 $\pm$ 0.2	1.2 $\pm$ 0.3
<b>Small intestine</b>	0.8 $\pm$ 0.5	1.3 $\pm$ 0.8
<b>Large intestine</b>	0.5 $\pm$ 0.1	0.7 $\pm$ 0.2
<b>Kidneys</b>	2.1 $\pm$ 1.3	4.2 $\pm$ 1.2
<b>Muscle</b>	0.4 $\pm$ 0.1	0.4 $\pm$ 0.3
<b>Bone</b>	4.3 $\pm$ 1.0	2.7 $\pm$ 0.5
<b>Skin</b>	2.1 $\pm$ 0.6	1.4 $\pm$ 0.5
<b>Tail</b>	1.3 $\pm$ 0.2	2.2 $\pm$ 1.2

**SUPPLEMENTARY TABLE 5.** Biodistribution data collected 144 h after the intravenous administration of [<sup>89</sup>Zr]Zr-DFO- $\alpha$ CD133 [3.7 -3.9 MBq, 10-10.5  $\mu$ g, in 100  $\mu$ L of PBS] or [<sup>89</sup>Zr]Zr-DFO-hIgG<sub>1</sub> [3.3-3.5 MBq, 36-38  $\mu$ g, in 100  $\mu$ L of PBS] to athymic nude mice bearing subcutaneous H82 xenografts (n = 4 per cohort). The data are presented as mean  $\pm$  standard deviation.

## REFERENCES

1. George J, Lim JS, Jang SJ, et al. Comprehensive genomic profiles of small cell lung cancer. *Nature*. 2015;524:47-53.